2012

Controlling and Understanding Self-Assembly

Olivia Hendricks
Wellesley College, ohendri2@wellesley.edu

Controlling and Understanding Self-Assembly

Olivia L. Hendricks
Advisor: Nolan T. Flynn, Chemistry

Submitted in Partial Fulfillment of the
Prerequisite for Honors in Chemistry

May 2012

Abstract

The ability to control the assembly of molecules on the nanometer scale is behind myriad technological innovations ranging from corrosion protection to cancer detection. One such assembly method is the formation of self-assembled monolayers (SAMs), or single molecular layers that spontaneously arrange on a surface. This thesis investigates the composition and redox properties of electroactive SAMs on planar and nanoparticle substrates. It incorporates work from two related projects:

1. *Creating electrochemically active nanoparticles (NPs)*

Several attempts to create electrochemically active NPs were explored, including place-exchange, codeposition, phase transfer, and organic coupling chemistries. Mixed monolayers of H_2Q-SH and thioctic acid (TA) were formed on the surface of AuNPs using place-exchange or codeposition reactions. These methods failed to deposit significant H_2Q-SH. Phase transfer of AuNPs into pure ethanol produced particles with electrochemical activity; however significant particle adsorption to the electrode surface occurred, preventing quantitative analysis. Amine-thiol and amine-carboxy coupling reactions were also performed on amine-functionalized polystyrene spheres (PS-NH_2s) in order to tether a hydroquinone moiety to the surface of these spheres.

2. *Exploring the kinetics of electron transfer in electrochemically active mixed monolayers*

Mixed monolayers were prepared using redox active hydroquinone-terminated alkanethiol (H_2Q-SH) and inert alkanethiols. The identity of the inert alkanethiol was varied to observe the effect of alkanethiol chain length on monolayer composition and electron transfer kinetics. Place-exchange studies with H_2Q-SH on monolayers of dodecanethiol (DT), octanethiol (OT), and hexanethiol (HT) were performed. The resulting monolayers were characterized using cyclic voltammetry and chronoamperometry. As the length of the inert alkanethiol decreased, the exchange rate increased and the fraction of H_2Q-SH in the monolayer increased.

Acknowledgments

First, I want to thank my advisor **Nolan Flynn** for his infinite support over the past three years. It feels like just yesterday that I joined your lab, a terrified first year feeling incredibly overwhelmed by the prospect of independent research. Your guidance and willingness to teach allowed me to take ownership of my research in a way that I never imagined possible. You have given me so many opportunities, and I thank you for your encouragement, your thoughtfulness, and of course, your "acerbic wit." You have made me into the chemist that I am today.

I would also like to thank my committee members **Carla Verschoor**, **David Haines**, and **Courtney Lannert.** Dr. V, since the very beginning, you made the chemistry department my "home away from home." Thank you for your honest advice and support. I could not have written this thesis without you! Professor Haines, thank you for your insightful questions and your willingness to help with my research. Your office door was always open when I needed to talk about organic chemistry, research, or life after Wellesley. I am so grateful for your input and advice on this thesis. Professor Lannert, you have always gone above and beyond expectations, both in helping me with physics and in being a part of this research since the fall. Thank you for all of your help! I would also like to thank **Rein Kirss** for allowing me to work on several of his projects and for teaching me about transition metal chemistry.

To all of the Flynn lab members, past and present, you guys are the best! To my fellow thesis-ers **Allison Yee** and **Lisa Jacob**, I have truly enjoyed working with you both. I can't imagine sharing my last year in Flynn lab with a better group of seniors! **Steph Schmitt** (aka Schmickle), thank you for making Flynn lab so much fun. Your constant cheerfulness and unfailing kindness never cease to amaze me. **Maddie Vara**, thank you for always staying in touch. I've enjoyed hearing about your adventures at NanoTerra, and I always appreciate your advice!

Katie Foley, Shoshana Bachman, Jasmine Rana, Emma Nechamkin, Liz Lawler, Ashton Vattelana, Kristen Hobbs, Christina Scavuzzo, Katie Pavia, **Steph Schmitt, Nadia Chaudhry-Waterman,** and **Lucy Archer**, thank you for being the best group of friends I could have asked for. Our regular breakti/lunch/dinner dates hold some of my favorite Wellesley memories. I feel incredibly fortunate to know such amazing people! Stay in touch!

I would also like to acknowledge the Jerome A. Schiff Fellowship, the Howard Hughes Medical Institute, the Sherman-Fairchild Foundation, and the Camille and Henry Dreyfus Foundation for supporting this research.

Finally, I would like to thank my amazing family. **Mom** and **Dad**, thank you for supporting me in every possible way. Words cannot describe how grateful I am for the opportunities you have given me. Thank you for always believing that I could achieve my goals. **Lynn Taylor**, you are the reason that I went to Wellesley. Your support, encouragement, and advice have meant so much to me over the years. Thank you for everything! **Kristen Newton** and **Cindy Ferguson**, thank you for always welcoming me back to Rocking Horse Farm. It has kept me sane! Because of you, horseback riding will always be a part of my life.

I would like to dedicate this thesis to Rosie.

1 INTRODUCTION

Technological innovations ranging from electronic devices to medical diagnostics rely on the directed assembly of molecules on the nanometer scale. One such assembly method is the formation of self-assembled monolayers (SAMs), or single molecule layers that spontaneously arrange on a metal surface to form ordered structures.[1] An extensively studied class of SAMs is alkanethiols adsorbed on gold.[2] Gold is an ideal metal because it is relatively inert and does not form stable oxide surfaces. In addition, the strong specific interaction between gold and sulfur allows monolayers to form in the presence of other functional groups.[1] As shown in Figure 1, alkanethiols assemble on both planar[2] and nanoparticle[4] substrates. Such assemblies have been

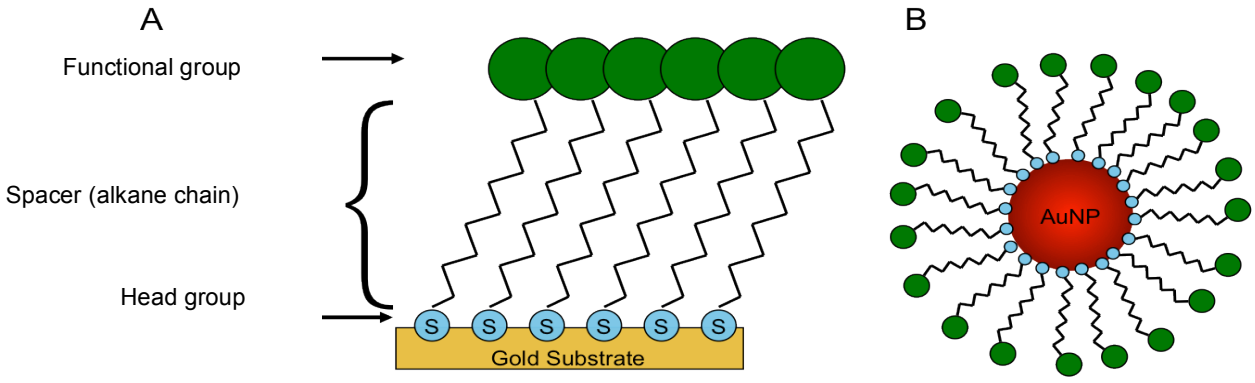

Figure 1: SAM on a planar gold substrate (A) and on a gold nanoparticle (B)

used in myriad applications ranging from the kinetics of electron transfer,[3] to the detection of toxic heavy metals in water systems,[4] to the diagnosis of lung cancer.[5] Our objective is to investigate the composition and electronic properties of mixed monolayers, where one of the molecules composing the SAM possesses an electrochemically active functional group. To this end, we will incorporate work from two related projects.

1. Exploring the kinetics of electron transfer in electrochemically active mixed monolayers

2. Creating electrochemically active nanoparticles for an electrochemically triggered assembly method of nanoparticles

1.1 SELF-ASSEMBLED MONOLAYERS

1.1.1 Self-Assembled Monolayers on Planar Substrates

SAMs lower the interfacial free energy between the metal surface and its environment. Figure 2 shows a more detailed structure of a typical SAM on a planar gold substrate. The sulfur binds to the gold by chemisorption with a bond strength of approximately 200 kJ/mol. However, the mechanism of bond formation remains contested. The alkanethiols are gauche to one another and are canted by 30°.[1]

SAMs are typically prepared by immersing a metal substrate in a dilute ethanolic solution of thiols at room temperature.[6] Dense coverage is achieved in milliseconds to minutes, but a slow reorganization process requires hours to maximize density and minimize defects. Immersion time, solvent, temperature, concentration, structure of the adsorbate, cleanliness of the surface, and concentration of oxygen all affect the rate of SAM formation.[1]

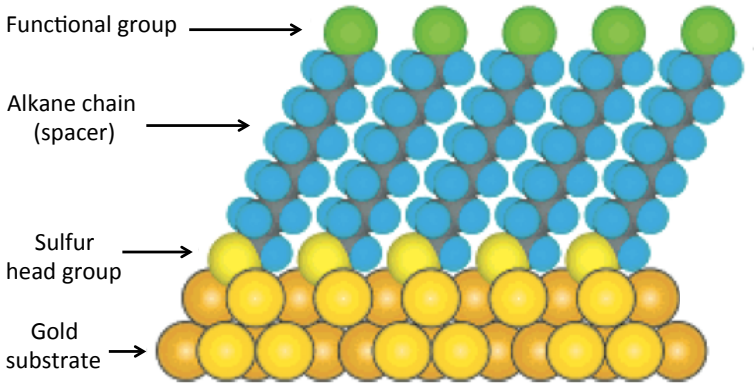

Figure 2: Diagram of an SAM assembled on a gold surface. Alkanethiol chains are canted by 30° and the chains are rotated 90° with respect to one another.

Using more than one type of alkanethiol, it is also possible to prepare mixed SAMs. Studies have shown that these mixed SAMs are homogeneous.[7,8] In other words, discrete phase segregation does not occur, despite variations in the functional group or chain length. Mixed SAMs are useful for

tuning the chemical properties of a surface or in establishing a chemical gradient along an interface. They are typically prepared by codeposition, place-exchange, or adsorption of asymmetric dialkylsulfides or disulfides. For codeposition, the substrate is simply immersed in a mixture of thiols. The mole fraction of a specific adsorbate in the SAM is directly related to the mole fraction of the adsorbate in the solution. However, the composition of the mixed monolayer rarely mirrors that of the solution. Factors such as solvent, functional groups, and relative chain lengths all affect monolayer composition. For example, in a mixture of two alkanethiols, a more polar solvent will favor the adsorption of the less polar species.[7] In addition, longer chains are preferentially adsorbed because of stronger London dispersion forces among adjacent molecules in the monolayer.[8] These same factors influence the composition of mixed monolayers formed through place-exchange.[9] In this method, a fully equilibrated monolayer is immersed in a solution containing a second alkanethiol. The second alkanethiol displaces some of the original monolayer, initially at defect sites and more slowly at crystalline-domain sites.[9]

The use of asymmetric disulfides and dialkylsulfides is less prevalent than place-exchange and codeposition of thiols. The composition of a SAM from disulfides is often difficult to control, as it frequently deviates from the expected 1:1 stoichiometry of the precursor molecule. Furthermore, disulfides are usually less soluble than the corresponding thiols. Asymmetric dialkylsulfides are advantageous because they remain intact upon adsorption. However, they have a much weaker interaction with gold. As a result, alkanethiols are the most commonly employed method for assembling SAMs on gold substrates.

1.1.2 Self-Assembled Monolayers on Nanoparticle Substrates

Just as they adsorb to planar substrates, alkanethiols also adsorb to gold nanoparticles (AuNPs) through a similar mechanism.[10] SAMs improve the stability of AuNPs in solution by acting as a physical and/or electrostatic barrier to aggregation.[11] For example, AuNPs were functionalized with mercaptoalkanes possessing ionizable functional groups. This increased the electrical double layer repulsion among particles, an effect that increased with SAM thickness.[10]

The structure of NP SAMs depends on the size of the NP. Smaller NPs have a higher radius of curvature. As a result, the chain density decreases farther from the NP core for these small NPs. Measurements of the hydrodynamic radii of functionalized NPs confirm this theory. The measured hydrodynamic radius is consistently less than the radius of the core plus the length of the fully extended alkanethiol. This suggests that the monolayer is loosely packed along the outer edge.[1] However, for the NPs used in this research ($\geq$ 11.2 nm in diameter), the surface behaves like that of a planar substrate.[1]

There are several ways to form a SAM on the surface of a nanoparticle (NP). These include synthesizing particles in the presence of thiols, covalent modification of existing ligands, and the familiar methods of codeposition and ligand exchange. Synthesizing NPs in the presence of alkanethiols can afford greater flexibility in the choice of solvent. For example, AuNPs in dichloromethane have been prepared by reducing a gold salt in the presence of dodecanethiol.[12]

1.2 ELECTROCHEMICAL TECHNIQUES

Characterizing the resulting SAMs is essential for furthering our understanding of these materials. Cyclic voltammetry (CV) and chronoamperometry (CA) are useful techniques for studying the structure, composition, and electrochemical properties of SAMs. In CV, current is

measured as a function of applied electrical potential. CV can be performed on free molecules in solution or on a SAM coating the electrode surface, and it is ideal for studying coupled electrochemical-chemical reactions.[25] For example, CV was used to investigate the kinetics of a Diels-Alder reaction. Researchers in the Mrksich group formed a SAM of 2-mercaptobenzoquinone on the surface of a gold electrode. They scanned over a potential range to oxidize the terminal hydroquinone (H_2Q) to the corresponding benzoquinone (BQ). The BQ was then available for a Diels-Alder reaction with free cyclopentadiene in solution.[13] By plotting the peak current as an exponential function of time, they were able to extract the first and second order rate constants for this reaction. The rate of this interfacial reaction differed significantly from the analogous reaction in solution. It did not follow a second-order kinetic pathway. Instead, the data were consistent with a mechanism by which the cyclopentadiene adsorbs to the surface of the electrode prior to reacting with the immobilized dienophile. In a subsequent study, they explored how the kinetics of the same reaction depended on the environment of the immobilized H_2Q.[14] In a mixed monolayer of 2-mercaptobenzoquinone and hydroxyl-terminated alkanethiol, the kinetics of the reaction were consistent with a traditional bimolecular reaction in solution. When the hydroxyl groups were replaced with methyl groups, however, the kinetic pathway returned to that of the pure benzoquinone monolayer. Given its utility in analyzing surface reactions on planar substrates, CV will be ideal for studying analogous reactions on the surface of AuNPs.

CA is a related technique in which current is measured as a function of time. However, instead of continuously varying the potential (as in CV), discrete potential steps are taken. The current decay is measured following each potential step. Integrating the current over time yields the total amount of charge passed during the reaction. As a result, CA has been used to quantify

the amount of electroactive species present in a SAM.[9,20,22] Furthermore, rate constants for electron transfer can be extracted by linear regression of the current decay.[3] Combined, CA and CV are ideal for studying the composition and electron transfer kinetics of mixed monolayers.

1.3 ELECTRON TRANSFER IN ELECTROACTIVE MIXED MONOLAYERS

Electron transfer is a ubiquitous process with applications ranging from the bioenergetics of photosynthesis to electronic devices. As a result, a fundamental understanding of nanoscale charge transfer is essential. SAMs are an easy way to study the kinetics of electron transfer. Their ordered, two-dimensional structure creates charge-transfer bridges at fixed donor-acceptor distances. In addition, the ability to selectively induce surface reactions represents the next step in SAM development.[15] Electroactive SAMs are ideal for this purpose, as it is possible to trigger a chemical reaction by applying an electrical potential. In this way, "static" SAMs can be transformed into dynamic surfaces with adjustable physical, chemical, and biological properties.

1.3.1 Applications

Biological Activity

Electroactive SAMs have been used to control the binding of biological molecules. Researchers in the Mrksich group created a substrate that selectively activated ligands for cell migration and

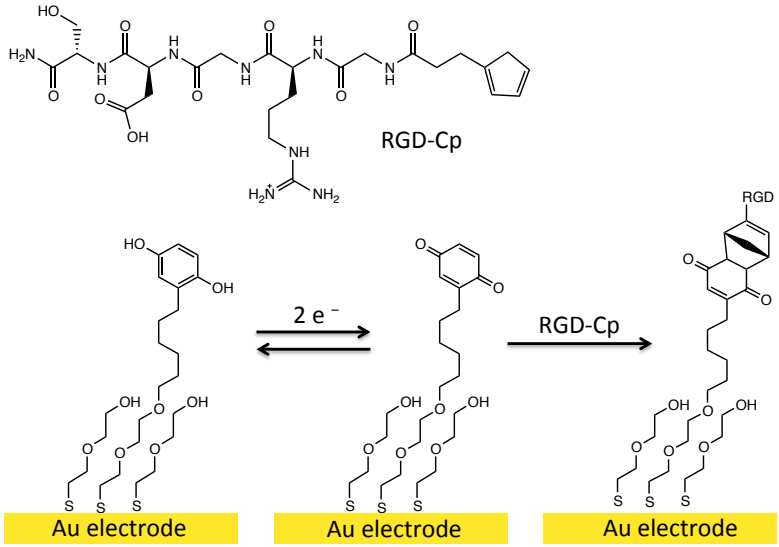

Figure 3: Electrochemically-triggered introduction of RGD peptide by a Diels-Alder reaction.

proliferation.[16] As shown in Figure 3, the substrate was based on a SAM possessing terminal hydroquinone (H_2Q) groups on a background of penta(ethylene glycol). When an electrical potential was applied to the gold substrate, the H_2Q was oxidized to BQ. Only the resulting BQ was available for a Diels-Alder reaction with a cyclopentadiene and Gly-Arg-Gly-Asp-Ser-NH_2 conjugate (RGD-Cp). Because the diene moiety was tethered to the RGD ligand, the Diels-Alder reaction immobilized the peptide on the electrode surface. RGD is known to promote cell adhesion, and researchers demonstrated that cell attachment was mediated by immobilization of this ligand. Thus, they created a surface that could be electrically switched from a state that prevented cell adhesion to a state that promoted it.

In addition, researchers used electrochemistry to trigger a bioactive biotin surface.[17] As shown in Figure 4, the electrode was functionalized with a biotin derivative containing a H_2Q moiety. After oxidizing H_2Q to the corresponding BQ, nucleophilic acyl substitution by water resulted in the release of BQ along with CO_2. This left an activated biotin surface that was available to bind with a variety of biological molecules, including streptavidin. Using this method, they developed a protein micropatterning technique based on electrochemistry.

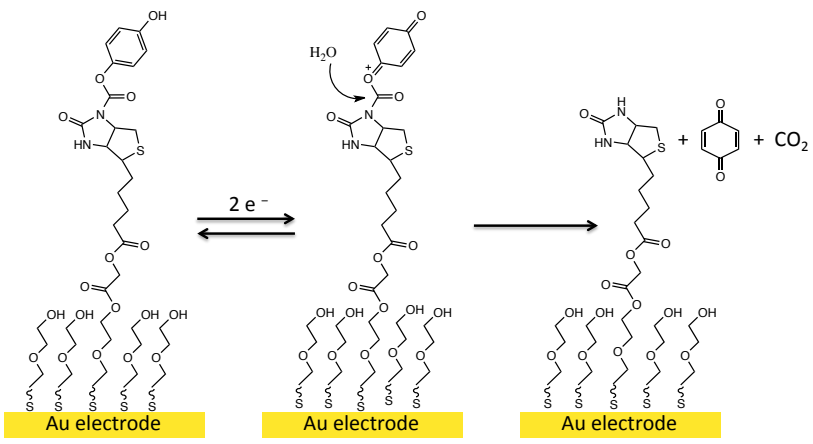

Figure 4: Electrochemically-triggered bioactive biotin surface.

Chemical Catalysis

Instead of activating surface-bound reactants, Chidsey, Collman, and co-workers electrochemically activated a copper (I) catalyst for the Huisgen 1,3-dipolar cycloaddition, also known as Sharpless "click" chemistry.[18] As shown in Figure 5, a mixed SAM containing azidoundecanethiol was assembled on the surface of a gold electrode. Cyclic voltammetry was performed to reduce copper (II) to copper (I) in the presence of ethynyl ferrocene. Reduction of the copper catalyst initiated the alkyne-azide "click" reaction to form a triazole ring. By tethering the alkyne to a ferrocene group, researchers could electrochemically monitor the extent of this reaction over time. This work demonstrated the applications of electrochemistry to chemical catalysis. Furthermore, because the surface-bound reactants were not electrochemically active, it increased the design flexibility in tailoring surface reactions.

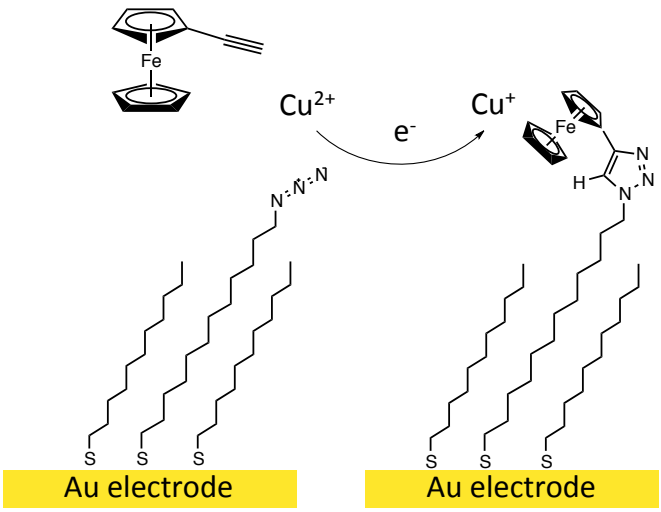

Figure 5: Electrochemically-triggered catalysis of "click" chemistry.

Molecular Electronics

SAMs have gained considerable attention for their use in molecular electronics. Researchers synthesized novel dithiazepane-functionalized ferrocenyl-phenylethynyl oligomers in order to study their redox behavior.[19] Their molecular structure is shown in Figure 6. These molecules adsorbed to the surface of a gold electrode following cleavage of the disulfide bond. This resulted in bipodally anchored electroactive SAMs. CV of the resulting SAMs yielded ideal

behavior with minimal peak separation or asymmetry. As a result, these molecules were promising candidates for molecular wires.

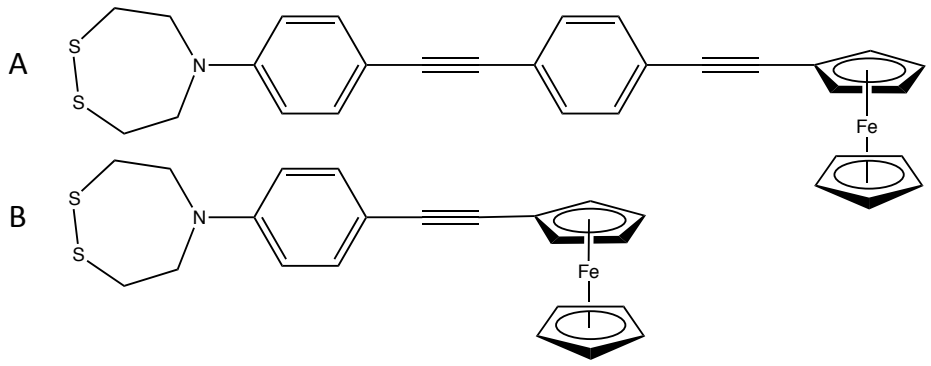

Figure 6: Dithiazepane-functionalized ferrocenyl-phenylethynyl oligomers **A** and **B.**

1.3.2 Previous Studies of Electrochemically Active Self-Assembled Monolayers

Structure and Exchange Kinetics of Electroactive Self-Assembled Monolayers

Electrochemically active SAMs have been used to probe the detailed structure of organic monolayers. Researchers performed a series of exchange experiments in which inert alkanethiols were replaced with electrochemically active ferrocene-terminated thiols.[20] Conversely, the ferrocene-terminated thiols were replaced with inert alkanethiols. Cyclic voltammetry was performed on the resulting SAMs to determine the ferrocene surface charge density in each monolayer. In both cases, significant exchange was observed within the first few hours. At longer time points, the composition of the monolayer slowly trended towards that of an intermediate monolayer obtained with a bare gold electrode. In addition, the more time that was allowed for exchange, the greater the peak separation. Finally, while increased peak splitting was observed when ferrocene-terminated thiols were replaced with unsubstituted thiols, this was not observed in the complementary experiment. Combined, these results confirmed that the equilibration process is multiphasic. A small fraction of thiols are easily exchanged, while the

rest are slowly exchanged, if at all. The thiols that are easily exchanged occupy defect sites in the monolayer. Slow exchange corresponds to thiols residing in the bulk domain of the monolayer, where tighter crystalline packing makes desorption less likely. Electron transfer is mediated by alkanethiols occupying these defect sites. At short times, the ferrocene-terminated thiol is exchanged primarily at defect sites. This results in very small peak separation, as the rate of electron transfer is faster than the scan rate. At longer exchange times, however, the ferrocene-terminated thiol begins to occupy sites within the crystalline domain. At these structurally well-defined areas, the ferrocene groups are held away from the electrode surface. As a result, the rate of electron transfer decreases to a rate that can be measured electrochemically. When a monolayer containing ferrocene-terminated thiols undergoes exchange with unsubstituted thiols, peak separation increases because the unsubstituted thiols replace ferrocene-terminated thiols at defect sites, eliminating the mediated path for electron transfer. Overall, electrochemical techniques were used to probe the structure of SAMs, demonstrating that exchange occurs primarily at defect sites followed by slower exchange in bulk domains.[20]

Composition of Electroactive Self-Assembled Monolayers

The composition of mixed monolayers resulting from place-exchange was examined using electrochemical techniques. In one study, researchers measured the place-exchange kinetics of a mixed monolayer containing a ferrocene-terminated thiol with an unsubstituted thiol. Many of their observations were qualitative, as the monolayer composition depended on solvent, chain length, thiol concentration, and the surface-density of the substituted thiol.[21] However, shorter alkanethiols were more easily exchanged, and solvents that assisted in the desorption process increased exchange efficiency.[21] In addition, the researchers observed that the

exchange process was not entirely reversible. Thiols adsorbed during an exchange reaction enter the monolayer at defect sites, and while most of these thiols were subsequently re-exchanged, a certain portion was not. This indicates that there is a process by which defect sites are converted into non-exchangeable crystalline domains. While defect sites resulting from the underlying gold substrate are permanent, defects resulting from impurities and packing imperfections can diffuse throughout the monolayer. This slow process of diffusion is responsible for the equilibrium between two different populations of surface bound thiols: those that can be exchanged, and those that cannot.[21]

Similar studies were performed exploring the composition of mixed monolayers resulting from codeposition reactions. Mixed monolayers of H_2Q-terminated octanethiol with unsubstituted alkanethiols were prepared on the surface of a gold electrode. The surface density of H_2Q was determined using cyclic voltammetry.[22] In this case, the composition of the mixed monolayer was highly dependent on the length of the unsubstituted alkanethiol chain. Only for hexanethiol did the composition of the mixed monolayer reflect the mole fraction of species in solution. Because hexanethiol is shorter than the H_2Q species, the two components interacted favorably in a closest packed pattern. As a result, adsorption is not significantly favored for one species over the other. In fact, at low H_2Q concentrations, there was an apparent overrepresentation of H_2Q-terminated octanethiol in the monolayer, most likely a result of favorable π-stacking between neighboring aromatic rings of the H_2Q species. As the chain length of the unsubstituted thiol increases, however, the linear relationship between solution composition and monolayer composition disappeared. The amount of hydroquinone present in the monolayer was significantly lower. In this case, the bulkiness of the hydroquinone functional group disrupted the crystalline packing, making its incorporation into the monolayer less

favorable. Overall, both the solution composition and the relative chain lengths of the two adsorbing species were significant in determining the composition of a mixed monolayer formed by codeposition.

Kinetics of Electron Transfer in Electroactive Self-Assembled Monolayers

Finally, electroactive SAMs were used to study the kinetics of electron transfer. As shown in equation 1, the rate constant for electron transfer, k_{ET}, depends exponentially on the distance between the electron donor and acceptor. k_0 is a preexponential factor, $d_{D,A}$ is the distance separating the donor and acceptor, and β is a structure-dependent attenuation factor describing the extent of electronic coupling between the electron donor and acceptor.

$$k_{ET} = k_0 e^{-\beta d_{D,A}} \qquad (1)$$

The value of β depends on the molecular structure of the bridge. For alkanethiols, the value of β typically lies between 0.9 and 1.3 $Å^{-1}$.[23]

H_2Q-terminated SAMs have been used to study the effect of alkyl chain length on electron transfer kinetics.[24] As the length of the alkyl chain increased, the peak separation, ΔE_p, increased significantly. The electron was forced to travel a longer distance to reach the redox center, corresponding to a decrease in the rate of electron transfer. Using the data from these SAMs, researchers calculated a β value of 1.04 ± 0.06 $Å^{-1}$ per CH_2 group, which agreed with literature values for other electroactive SAMs.

1.3.3 Electroactive Mixed Monolayers

Despite the extensive study of electroactive SAMs, there has not been significant exploration of electron transfer kinetics in mixed monolayers. Specifically, the possibility of

intermolecular electron transfer has not been investigated. When the unsubstituted alkanethiol is significantly shorter than the electroactive alkanethiol, we propose a path for electron transfer that involves tunneling down the shorter alkane to reach the redox center. This path is shown in Figure 7. To test this hypothesis, we will create a series of mixed monolayers containing H_2Q-terminated dodecanethiol (H_2Q-SH) and unsubstituted alkanethiols of equivalent or shorter chain length, such as dodecanethiol (DT), decanethiol (dT), octanethiol (OT), and hexanethiol (HT).

We will use the previously discussed place-exchange method to create our electroactive mixed monolayers. After forming a pure monolayer of the unsubstituted alkanethiol, H_2Q-SH will be exchanged over the course of 72 hours. To limit inhomogeneities in the monolayer, we will back-fill with unsubstituted thiol. This will help to ensure that the H_2Q-SH occupies equivalent sites within the monolayer. Cyclic voltammetry and chronoamperometry will be used to study the composition and electron transfer kinetics of the resulting mixed monolayers.[25]

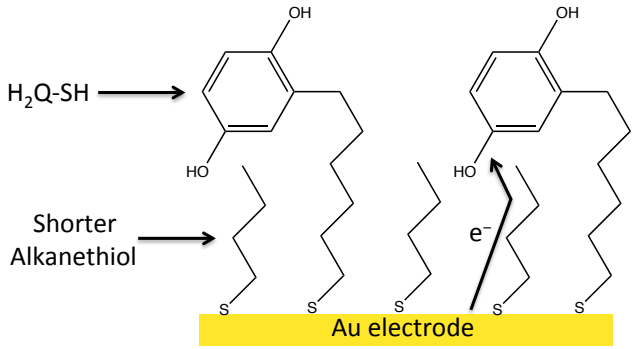

Figure 7: Mixed monolayer on the surface of a gold electrode demonstrating intermolecular electron transfer.

1.4 ELECTROCHEMIALLY TRIGGERED ASSEMBLY METHOD OF NANOPARTICLES

NPs exhibit unique, size-dependent optical, electronic, and magnetic properties. The directed assembly of NPs is of fundamental interest for applications in biosensing and optoelectronics. To date, several methods for NP assembly based on biomolecular recognition have been reported.[35,36,37] The dependence on biological molecules, however, places limitations

on reaction conditions. As a result, we propose a new, potentially more useful method for the assembly of nanoparticles, namely electrochemistry. This method does not require biological molecules, and it exploits the versatility of electrochemical techniques.

1.4.1 Applications

Chemiresistors

Chemiresistors are devices whose electrical resistance changes in the presence of chemical species.[26] Charge transport through nanoparticle-based chemiresistors depends on particle size, interparticle spacing, and the dielectric properties of stabilizing ligands.[27] As a result, the charge transport properties of these devices can be tuned by modifying the structure of surface ligands. Nanoparticle chemiresistors have been used in the diagnosis of lung cancer.[28] Researchers identified a series of biomarkers that were present in the exhaled breath of patients with lung cancer at different concentrations than healthy patients. AuNPs functionalized with alkanethiols acted as chemiresistors to detect the presence of these volatile organic molecules. Patients breathed into a custom apparatus that directed their breath over the AuNP chemiresistor. The resistance of the device changed significantly compared to the changes observed with the breath of healthy individuals. This proved to be a simple and reliable test for the diagnosis of lung cancer.

Ion Detection

Nanoparticle assemblies have also been used to detect metal ions in solution. For example, researchers developed an electrochemical sensor for oxyanions using AuNPs functionalized with (amidoferrocenyl)alkanethiol. The AuNPs were electrochemically active,

and it was possible to monitor the redox potential of the amidoferrocenyl moiety using cyclic voltammetry.[29] Oxyanions such as $H_2PO_4^-$ complexed to the amidoferrocenyl group, resulting in the appearance of a new, cathodically shifted wave. Therefore, a change in the redox potential of the functionalized AuNPs was used to detect the presence of oxyanions in solution.

Researchers were also able to spectroscopically detect heavy-metal ions in solution. AuNPs exhibit a surface plasmon resonance near 520 nm. Upon aggregation, this resonance maximum shifts to longer wavelengths.[30] Researchers took advantage of this property to detect metal ions that are "spectroscopically silent." AuNPs were functionalized with terminal carboxylic acid groups. In the presence of metal ions, a chelation process caused the aggregation of AuNPs in solution.[31] The color of the solution changed from wine red to a dark blue or purple, and this change was monitored using ultraviolet-visible absorption (UV-vis) spectroscopy. Addition of ethylenediaminetretaacetic acid (EDTA), which had a stronger affinity for the metal ions, reversed aggregation and restored the AuNP solution to its original color. Thus, the presence of metal ions in solution was monitored by a simple color change.

Molecular Recognition

In addition to ion sensing, nanoparticle assemblies have been used for molecular recognition. Two broad categories of electrochemical sensors are defined based on the location of the response. Exo-active sensors generate a response at the ligand-solution interface on the surface of the nanoparticle. Core-based sensors generate a signal in the nanoparticle core.[32]

Exo-active nanoparticle sensors were used to detect π-donor molecules.[33] A monolayer of AuNPs was / on an indium tin oxide (ITO) substrate using (3-amino-propyl)trimethoxysilane. The resulting AuNP layer was treated with cyclobis(paraquat-p-phenylene) (CPP), and

subsequent AuNP layers were deposited. CPP acts as a host for π-donor compounds such as H_2Q, which can be detected electrochemically. Ultimately, the researchers were able to detect the presence of free H_2Q at a concentration of 2–3 μM. The same concentration of H_2Q elicited no response with a bare electrode.

A similar device was incorporated into an ion-sensing field effect transistor (ISFET). AuNPs functionalized with CPP were deposited on the insulator of an ISFET. Upon addition of adrenaline, a π-donor compound, changes in the source-drain current were monitored. Similarly, changes in the gate-source voltage were monitored for a constant source-drain current and voltage. Based on these results, their limit of detection for adrenaline reached 1 μM.

Core-based AuNP sensors were used in the detection of DNA.[34] Target DNA was immobilized on the inside of a polystyrene microwell. AuNPs functionalized with the complimentary strand of DNA were introduced to the sample. Selective hybridization occurred, immobilizing AuNPs in the microwell. An acidic bromine-bromide solution was added to digest the gold particles, and anodic stripping voltammetry was used to quantify the amount of gold ions in solution. The limit of detection was 5 pM, which was significantly lower than other analytical techniques such as colorimetric detection or a quartz crystal microbalance.

1.4.2 Previous Methods of Nanoparticle Assembly

DNA-Based Assembly

DNA is a useful template for the directed assembly of AuNPs because of its ability to spontaneously form ordered secondary and tertiary structures. In one example of DNA-based assembly, AuNPs were functionalized with single-stranded DNA that had been modified with thiol groups.[35] Complimentary strands of DNA were synthesized to control the specific

orientation of the resulting AuNP assemblies. Figure 8 outlines the three synthesis strategies that were used in creating these AuNP assemblies. Briefly, the technique outlined in Figure 8A involved functionalizing AuNPs with complimentary strands of AuNPs to form double-stranded AuNP assemblies. In Figure 8B, AuNPs were assembled onto an unmodified template strand. In Figure 8C, AuNPs were positioned in a collinear arrangement by synthesizing two complimentary strands of DNA with either one or two incorporated thiol groups. The AuNPs were incorporated into a hybridized strand of DNA in order to avoid both thiol groups chelating to the same AuNP. Figure 9 shows representative transmission electron microscopy (TEM) images of AuNP assemblies prepared using the technique described in Figure 8A.

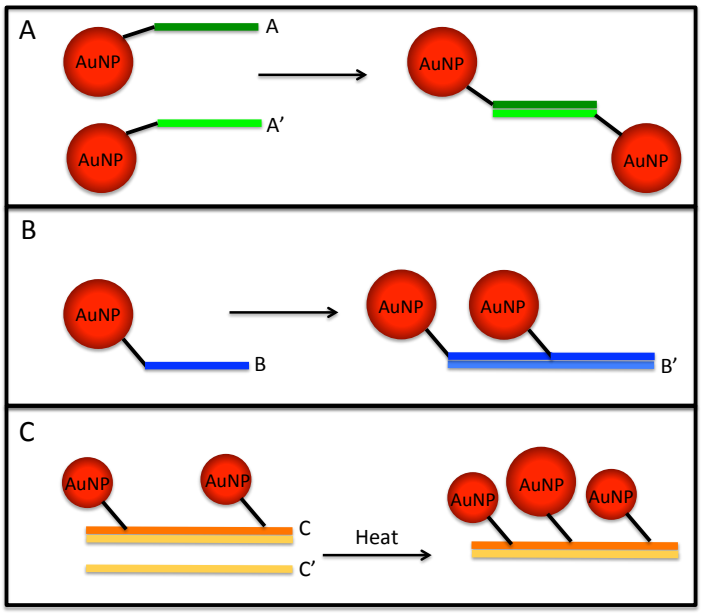

Figure 8: Synthetic strategies for DNA-based assembly of AuNPs. The letters A', B', and C' denote the complimentary strands to A. B, and C.

Figure 9: TEM images of AuNPs assembled using DNA base-pair recognition.

Biotin/Streptavidin-Based Assembly

The streptavidin/biotin system is ideal for nanoparticle assembly because of its high free energy of association for non-covalent binding between a protein and a small ligand. Furthermore, there are a wide variety of available biotin analogues, and the resulting complexes are stable over wide temperature and pH ranges. AuNPs were functionalized with a disulfide biotin analogue, and assembly was induced by the subsequent introduction of streptavidin.[36] The extent of assembly was monitored using dynamic light scattering (DLS), and the resulting assemblies were characterized using TEM and small angle X-ray scattering.

Coiled-Coil Peptide-Based Assembly

Coiled-coil peptides adopt a helical conformation that is stabilized by hydrophobic packing and side chain interactions between peptides. AuNPs were functionalized with two artificial peptides that together form these coiled-coil structures.[37] Upon mixing the two AuNP populations together, the peptides interact to form coiled-coils, resulting in the directed assembly of AuNPs in solution. Because of the basic side chains, assembly and disassembly were controlled as a function of pH. The extent of assembly was monitored using ultraviolet-visible spectroscopy (UV-vis), circular dichroism (CD) spectroscopy, and TEM.

Limitations

Despite the utility of these methods, the presence of biological molecules places limitations on the reaction conditions, such as temperature, solvent, pH, and ionic strength. While these limitations are sometimes exploited in controlling the assembly and disassembly of AuNPs in solution, future methods of AuNP assembly may require more universal conditions.

1.4.3 Electrochemically-Triggered Assembly

The goal of my research is to develop a new, more universal method for the directed assembly of NPs in solution. An electrochemical triggering method is ideal because of its applicability to a wide variety of conditions, ranging from *in vivo* studies to nonaqueous solvents.[25] To this end, we will create two populations of NPs. As shown in Figure 10, the first population (in red) is functionalized with a terminal H_2Q moiety, and the second population (in blue) is functionalized with a terminal aminooxy group. The terminal H_2Q undergoes a reversible redox reaction to the corresponding BQ, which will then spontaneously react with the oxyamine to form an oxime linkage.[38]

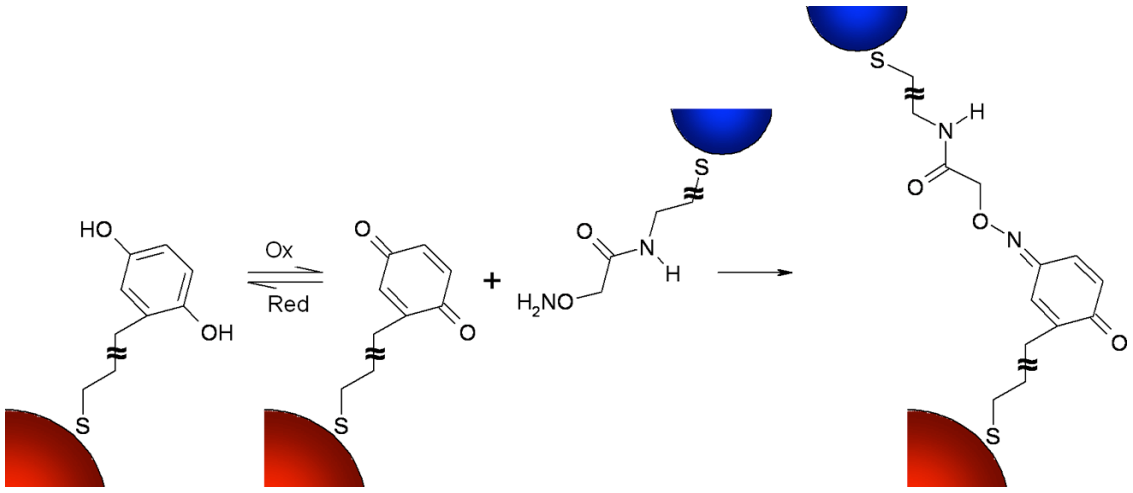

Figure 10: Reaction scheme of hydroquinone-functionalized NPs (red) coupling to aminooxy-functionalized NPs (blue) through the formation of an oxime bond.

Electrochemically-Triggered Surface Reactions

Electrochemically-triggered surface reactions on planar substrates have been extensively studied. As discussed in section 1.2, the first electrochemically-induced surface reaction was a Diels-Alder reaction of cyclopentadiene with immobilized 2-mercaptobenzoquinone.[13] Researchers also used electrochemistry to trigger the formation of an amide bond. They prepared

a SAM of 12,12'-dithiobis(dodecanoic acid hydroquinone monoester). Again, oxidation of the H_2Q moiety generated the corresponding BQ, which could act as a good leaving group. Nucleophilic acyl substitution with a primary amine formed an amide bond, and the extent of the reaction was monitored using cyclic voltammetry.

Most relevant to this work, however, was the formation of an oxime linkage using SAMs of H_2Q-SH.[38] Reaction of the oxyamine with BQ occurs in high yield at physiological pH and room temperature. The resulting oxime linkage is chemically stable and electrochemically active. Therefore, its formation was monitored not only by a decrease in the current wave for H_2Q, but also by an increase in the current wave for the oxime product.

Project Goals

Overall, our goal is to adapt the electrochemically triggered surface chemistry from planar substrates to a colloidal suspension of NPs. To this end, the immediate objectives of this project include:

1. Creating electrochemically active NPs
2. Using cyclic voltammetry to trigger the redox of the resulting NPs
3. Studying the electrochemical behavior with AuNPs of varying size

Electrochemically-Active Nanoparticles

Experimental trials with both AuNPs and polystyrene spheres (PSs) will be used to create electrochemically active NPs. AuNPs functionalized with H_2Q-SH will be prepared using a place-exchange or codeposition method with thioctic acid (TA). TA was chosen because it was shown to stabilize AuNPs for further functionalization with neutral, negative, and positively-

charged thiols.[39] Alternatively, other solvents for functionalization, such as ethanol, will be explored to favor the deposition of H_2Q-SH.[40] A new synthetic technique might also be explored that produces DT-capped AuNPs in dichloromethane. This strategy is attractive because dichloromethane is a convenient solvent for electrochemistry.[41] A place-exchange reaction would then be performed to replace some of the surface bound DT with H_2Q-SH. This method was used to prepare electrochemically active AuNPs with a ferrocene moiety.[29]

Amine modified PSs offer an alternative to AuNPs, as they possess a higher surface charge density that improves their stability in aqueous solution. The amine functionality on the surface of these spheres enables a variety of biochemical protein coupling techniques. For example, amine-thiol coupling is performed in aqueous solution using the commercially available coupling agent sulfosuccinimidyl-4-(*N*-maleimidomethyl)cyclohexane-1-carboxylate (sulfo-SMCC). Figure 11 depicts the coupling mechanism. The NHS ester reacts selectively with

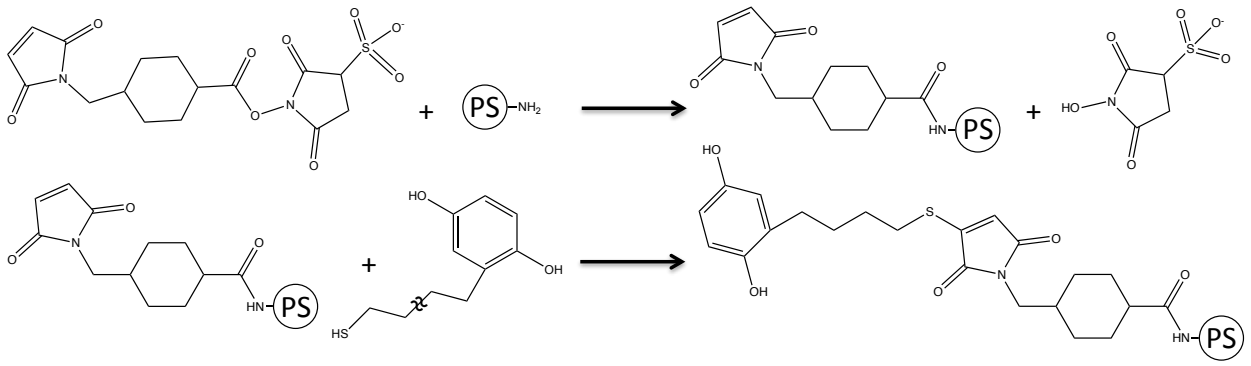

Figure 11: Amine-thiol coupling using sulfo-SMCC.

primary amines at pH 7–9 to form stable amide bonds. The malemide group reacts with thiols at pH 6.5–7.5. In this case, the cyclohexane bridge improves the stability at higher pH, and the sulfonyl moiety improves the solubility in water.

As an alternative to amine-thiol coupling with sulfo-SMCC, it is possible to couple primary amines to carboxylic acid functionalities using 1-ethyl-3-[3-dimethylaminopropyl]carbodiimide hydrochloride (EDC). H_2Q moieties are available with a carboxylic acid functional group ortho to the hydroxyl group (2,5-dihydroxybenzoic acid), making this an attractive option for coupling hydroquinone to the surface of the PS spheres. As shown in Figure 12, EDC reacts with a carboxyl to form an unstable amine-reactive *O*-acylisourea intermediate. In aqueous solvents, the addition of *N*-hydroxysulfosuccinimide (sulfo-NHS) stabilizes this intermediate by converting it to an amine-reactive sulfo-NHS ester. Addition of the primary amine results in the formation of a stable amide bond.

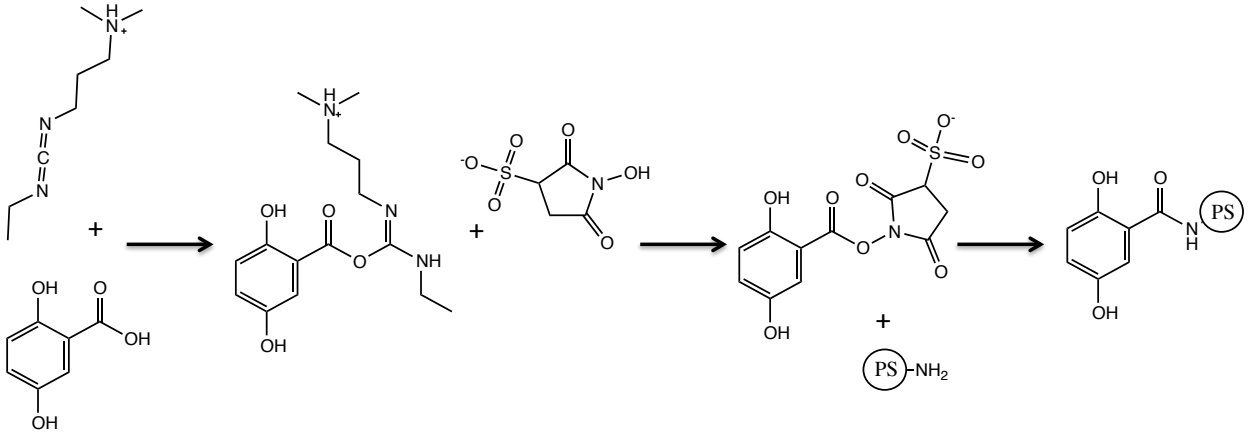

Figure 12: Amine-carboxy coupling using sulfo-NHS

Successful creation of these electrochemically active NPs would expand the toolkit available to scientists to control the assembly of NPs in solution. By varying the size of the electrochemically active NPs, fundamental studies of the diffusion of NPs in solution could be performed. Furthermore, this would be the first reported use of electrochemistry to trigger the assembly of NPs in solution. The versatility of electrochemistry would make this assembly method a more universal technique to enable coupling of a wide variety of nanostructures.

2 Materials and Methods

2.1 Materials

High purity water was used for all aqueous sample preparations and solutions (Thermo Scientific Barnestead EasyPure II Ultrapure Water Purification System, 18.2 MΩ cm). For all ethanolic solutions, 200 proof absolute anhydrous ethyl alcohol (ACS/USP grade, 99.98%) was purchased from PharmCo-AAPER (Brookfield, CT). Dichloromethane (HPLC grade, ≥ 99.8%) was purchased from EMD Chemicals (Gibstown, NJ). Potassium gold (III) chloride (99.995%) and sodium citrate tribasic dehydrate (ACS reagent ≥ 99.%) were purchased from Sigma-Aldrich (St. Louis, MO) for gold nanoparticle synthesis. 330 nm amine-functionalized polystyrene spheres (PS-NH_2) were initially purchased from Bangs Laboratories (Fishers, IN) and later from Magsphere Inc (Pasadena, CA).

For particle functionalization, (±)-α-Lipoic acid (thioctic acid, ≥ 99%) and 6-mercaptohexanoic acid (97%) were purchased from Sigma-Aldrich. Bis(*p*-sulfonatophenyl)phenyophosphine dehydrate dipotassium salt (≥ 97%) was purchased from Strem Chemicals (Newburyport, MA). Hydroquinone-terminated dodecanethiol (H_2Q-SH) was purchased from ProChimia (Sopot, Poland). Amino- and methoxy-terminated poly(ethylene oxide) (MW = 5300), carboxy terminated poly(N-isopropyl acrylamide) (MW = 10800), α-hydroxyl-ω-thiol terminated poly(ethylene oxide) (MW = 2300) and α-carboxyl-ω-thiol terminated poly(ethylene oxide) (MW = 2200) were purchased from Polymer Source (Quebec, Canada).

For coupling procedures, 1-ethyl-3-(3-dimethylaminopropyl) carbodiimide HCl, N-hydroxysulfosuccinimide, H-hydroxysuccinimide, and sulfosuccinimidyl-4-(N-

maleimidomethyl)cyclohexane-1-carboxylate were purchased from Thermo Scientific (Rockford, IL). Sodium carbonate monohydrate (≥99.5%) was purchased from Sigma Aldrich. PBS (0.010 M phosphate buffer, 0.50 M sodium chloride) at pH 7.2 was prepared from sodium phosphate dibasic (≥ 99.0%) purchased from EMD chemicals, potassium phosphate monobasic (≥ 99.0%) purchased from Sigma Aldrich, and sodium chloride (≥ 99.5%) purchased from Sigma Aldrich. MES buffer at pH 6 was prepared from 0.1 M 2-[*N*-morpholino]ethanesulfonic acid sodium salt (≥ 99%) and 0.5 M sodium chloride (≥ 99.5%) purchased from Sigma Aldrich. 6 M HCl from EMD Chemicals was used to adjust the pH. Dialysis tubing (nominal MWCO = 3500) was purchased from Fisher Scientific (Pittsburgh, PA).

For all electrochemical experiments, concentrated Omni*Trace* Ultra™ sulfuric acid (93–98%) from EMD Chemicals was used to prepare the supporting electrolyte (0.100 M H_2SO_4 unless otherwise noted). All glassware was cleaned using aqua regia, a 3:1 mixture of concentrated nitric acid (68–70.0%) from EMD Chemicals and concentrated hydrochloric acid (37%) from VWR International (Radnor, PA). Hydroquinone (99%) and 2,5-dihydroxybenzoic acid (98%) were purchased from Sigma-Aldrich. SAMs were formed using 1-dodecanethiol (≥ 98%), 1-decanethiol (96%), 1-octanethiol (≥ 98.5%), and 1-hexanethiol (95%) from Sigma-Aldrich. H_2Q-SH from ProChimia was also used in all electroactive monolayers.

2.2 Gold nanoparticle synthesis

AuNPs were synthesized according to the procedure outlined by Flynn and Gewirth.[42] Briefly, 50.00 mL of 1.00 mM potassium tetrachloroaurate solution was heated to reflux at 100°C. While vigorously stirring, 5 mL of a 38.8 mM trisodium citrate solution was quickly added. Within the first 5 minutes, the color of the solution changed from pale yellow to clear to

black and finally to wine red. The solution was stirred and refluxed for one hour and then cooled for 30 minutes. AuNPs were stored in the dark at ambient conditions.

2.3 Gold nanoparticle functionalization

2.3.1 Place-exchange method

AuNPs were functionalized with thioctic acid (TA) following a modified procedure by Jans et al.[43] First, 10 mL of a 1.0 M sodium hydroxide stock solution was added to 4.00 mL of AuNPs. This raised the pH of the AuNP solution above 11. TA was then added from a 10 mM ethanolic stock solution to reach a final concentration of 1 mM, 100 μM, 10 μM, or 1 μM. The solution was stirred overnight and was purified by centrifuging twice (SS-34 rotor) at 6,723 g and 10°C in 4.00 mL aliquots. The AuNPs were re-suspended in 4.00 mL nanopure water and re-dispersed using an ultra-sonic horn (5–10 seconds, continuous pulse, output = 2–3). The pH was adjusted again by adding 10 mL of 1.0 M NaOH to 4.00 mL of TA-functionalized AuNPs. H_2Q-SH was then added from a 10 mM ethanolic stock solution to reach a final concentration of 1 mM, 100 μM, 10 μM, or 1 μM. After stirring overnight, the particles were purified by centrifuging twice as previously described.

2.3.2 Codeposition method

The pH of a 4.00 mL AuNP solution was adjusted by adding 10 mL of a 1.0 M sodium hydroxide stock solution. TA and H_2Q-SH were added simultaneously from 10 mM ethanolic stock solutions. The final concentration of TA was 100 μM or 50 μM, and the final concentration of H_2Q-SH was 100 μM, 10 μM, or 1 μM. After stirring overnight, the particles were purified as described in section *2.3.1*.

2.4 Gold nanoparticle phase transfer

AuNPs were transferred into ethanol following the procedure by Han et al.[40] Briefly, 4 mL aliquots of AuNPs were centrifuged twice for 20 minutes at 5,992 g and 10°C. After the first wash, AuNPs were re-suspended in 4 mL nanopure wate. After the second wash, AuNPs were re-suspended in ethanol. The ultrasonic horn was used to re-disperse the particles after both wash cycles (see *2.3.1*).

2.4.1 Functionalization with hydroquinone-terminated dodecanethiol

H_2Q-SH was added directly to 4.00 mL of ethanolic AuNPs from a 10 mM ethanolic stock solution. The final concentration of H_2Q-SH was 1 mM or 100 μM. Alternatively, aqueous AuNPs were first functionalized with bis(*p*-sulfonatophenyl)phenyophonsphine dehydrate dipotassium salt (SPPP) at a concentration of 20 mM. After stirring overnight, 4 mL aliquots of AuNPs were centrifuged twice for 20 minutes at 5,992 g and 10°C. Each time, AuNPs were resuspended in nanopure water, and the ultrasonic horn was used to re-disperse (see *2.3.1*). The particles were centrifuged a third time at the same parameters and re-suspended in pure ethanol. The ultrasonic horn was used to re-disperse. H_2Q-SH was then added to 4.00 mL AuNPs for a final concentration of 1 mM or 100 μM. After stirring overnight, the particles were centrifuged twice at 19,414 g and 10 °C for 20 minutes, re-suspending in pure ethanol each time. Again, the ultrasonic horn was used to re-disperse.

2.5 Polystyrene Sphere Covalent Coupling

2.5.1 Amine-thiol coupling

Coupling between PS-NH_2 and various thiols was accomplished using sulfosuccinimidyl 4-[*N*-maleimidomethyl]cyclohexane-1-carboxylate) (sulfo-SMCC). The protocol was adapted from TechNote 205, Bangs Laboratories. Amine-terminated polystyrene spheres (PS-NH_2) were

suspended in PBS at 10% v/v. The samples were centrifuged twice at 3,360 g for 30 minutes and vortexed to re-disperse. After the first wash, the particles were re-suspended in PBS. After the second wash, they were re-suspended in 2 μM or 200 μM sulfo-SMCC in PBS. The samples were stirred for 30 minutes before centrifuging again at 3,360 g for 20 minutes. The samples were re-suspended in PBS at half of their original volume. The samples were then combined with a 1 mM stock solution of 6-mercaptohexanoic acid (MHA), α-hydroxyl-ω-thiol terminated poly(ethylene oxide), or α-carboxyl-ω-thiol terminated poly(ethylene oxide) to restore original volume. A 1 mM MHA stock solution was prepared in PBS from a 10 mM ethanolic MHA solution. The particle solutions were then stirred overnight and centrifuged according to the method described above.

2.5.2 Amine-carboxy coupling

N-hydroxysulfosuccinimide (sulfo-NHS) and 1-ethyl-3-[3-dimethylaminopropyl] carboiimide hydrochloride (EDC) were used to couple PS-NH_2 to 2,5-dihydroxybenzoid acid (DHB). A 200 mM DHB solution was prepared in 4.00 mL MES buffer. To this DHB solution, 1.5 mg EDC and 4.4 mg sulfo-NHS were added to reach final concentrations of 2 mM and 5 mM, respectively. The solution was stirred for 15 minutes, after which the pH was raised to ~7 by adding 0.02 g sodium carbonate. Next, 400 mL PS-NH_2 were added and the solution was stirred for two hours. The particles were then centrifuged twice at 3,360 g for 20 minutes, re-suspending in nanopure water and vortexing to re-disperse.

2.5.3 Controls to test coupling

Thermoresponsive polymer

The procedure described in 2.5.2 was used to couple PS-NH_2 to carboxy-terminated poly(N-isopropyl acrylamide) (polyNIPAM). The resulting samples were characterized by UV-

vis spectroscopy (see *2.6.1*). A Varian Cary PCB 150 water peltier system was used for temperature controlled spectra at 25°C and 45°C.

Dialysis tubing

DHB was coupled to amino- and methoxy-terminated poly(ethylene oxide) using the procedure outlined in *2.5.2*. After the reaction was complete, the solution was transferred to dialysis tubing and stirred overnight. The outer solution was refreshed after 24 hours, and the sample was stirred for an additional 24 hours. To ensure sufficient equilibration time, the presence of DHB in the outer solution was monitored using cyclic voltammetry (*2.8.1*). The coupled product was also characterized using cyclic voltammetry.

2.6 Nanoparticle Characterization

2.6.1 Ultraviolet-visible spectroscopy

Ultra-violet visible (UV-vis) spectra of all nanoparticle solutions were obtained using a Varian Cary 500 Scan UV-visible-NIR spectrophotometer (Santa Clara, CA). Absorbance spectra were collected from 350–800 nm using a plastic cuvette with a path length of 1 cm. All spectra were acquired in double beam mode with baseline correction using the appropriate solvent for baseline. Unless otherwise noted, samples were diluted by a factor of 10.

2.6.2 Dynamic light scattering

Particle size and polydispersity were measured using dynamic light scattering (DLS) on a Malvern Zetasizer Nano ZS (Worcestershire, UK), running Zetasizer Software 6.01. To collect spectra, 1 mL of sample suspended in water, PBS, or ethanol was placed in a plastic cuvette. AuNP samples were filtered using a 0.2 mm cellulose acetate syringe filter. For AuNPs suspended in water, the dispersant viscosity = 0.8872 cP and the refractivity index = 1.650. For

AuNPs suspended in ethanol, the dispersant viscosity = 1.2600 cP and the refractivity index = 1.650. For PS-NH_2 suspended in PBS, the dispersant viscosity = 0.8872 and the refractivity index = 1.590. Unless otherwise noted, the temperature was set to 25°C. The collection angle was 173°. Particle hydrodynamic diameter and polydispersity were obtained from the "Size distribution by number" report. Results were given as the mean value of 12 or more measurements.

2.7 Monolayer Formation

To form SAMs of 1-dodecanethiol (DT), 1-decanethiol (dT), 1-octanethiol (OT), and 1-hexanethiol, a cleaned and polished gold electrode was soaked overnight in a 2 mM ethanolic thiol solution. For place-exchange reactions, the electrode was then soaked in a 100 μM ethanolic solution of H_2Q-SH for five days (~120 hours). For backfilling of defect sites, the electrode was soaked in a 2 mM solution of the appropriate thiol for 24 hours. No efforts were made to exclude oxygen. Prior to any electrochemical measurements, the electrode was rinsed with nanopure water.

2.8 Electrochemical techniques

All electrochemical experiments were carried out using an Epsilon Systems potentiostat (Bioanalytical Systems, West Lafayette, IN). The reference electrode was an Ag|AgCl sat'd KCl electrode (0.197 V vs. SHE), and the counter electrode was a gold wire. A glassy carbon electrode (GCE, 3 mm diameter) or a gold microelectrode (1.6 mm diameter) was used as the working electrode. Prior to use, the GCE was polished using 0.05 mm alumina polishing paste. The gold microelectrode was polished using 0.05 mm alumina polishing paste followed by 3 mm diamond polishing paste. All solutions were deoxygenated with nitrogen gas for 20 minutes. Throughout the experiments, nitrogen gas continuously bathed the surface of all solutions.

2.8.1 Cyclic Voltammetry

The following parameters were used for all experiments. The initial potential was set to −350 mV, the switching potential to 900 mV, and the final potential to −350 mV. For experiments involving HT monolayers, the initial and final potentials were set to −300 mV. The number of segments was 2, the filter was 10 Hz, the quiet time was 2 seconds, and the sample interval was 1 mV. The full scale was chosen based on the current amplitude (typically between 100 mA and 1 mA). The scan rates for each experiment were 250, 150, 100, 75, 50, 25, and 10 mV/s.

2.8.2 Chronoamperometry

The following parameters were used for all experiments. The initial potential was −350 mV, the first potential step was 900 mV, and the second potential step was −350 mV. For experiments involving HT monolayers, the initial potential and the second potential step were set to −300 mV. The quiet time was 65 seconds, and the time for each step was 65 seconds. The sample interval was 50 microseconds, and the maximum number of points per step was 4,000. The full scale was adjusted based on the current amplitude (typically 100 mA or 10 mA).

3 Results and Discussion

3.1 Electrochemically-Active Nanoparticles

As discussed in section 1.4.3, two populations of NPs are needed for electrochemically-triggered assembly. NPs functionalized with H_2Q moieties undergo a reversible redox reaction, producing a BQ moiety that reacts with a second population of NPs bearing a terminal amino-oxy group. Current work has focused on the creation of electrochemically active NPs.

3.1.1 Electrochemically Active Gold Nanoparticles

Previous attempts to functionalize AuNPs directly with H_2Q-SH resulted in irreversible particle aggregation. Almost immediately after adding H_2Q-SH, AuNP solutions turned purple and a black precipitate formed. This precipitate was re-dispersed using the ultra-sonic horn. Particle instability was confirmed using UV-vis spectroscopy. UV-vis spectroscopy is a useful technique to monitor the broad absorption bands exhibited by some colloidal nanoparticles. The wavelength of absorption satisfies a resonance condition for the collective oscillation of electrons, called a surface plasmon resonance (SPR). The SPR depends on the size, shape, and dielectric environment of the nanoparticles.[30] Spherical AuNPs of about 10 nm in size display a single absorption band at 520 nm that shifts to longer wavelengths upon functionalization. For the size of the alkanethiols used in this work, shifts are typically 10 nm or less.[31] Larger shifts and peak broadening indicate particle aggregation, as the plasmon resonances of neighboring particles couple together.[44] UV-vis allows us to monitor both peak position and broadness. As a result, it is a useful measure of particle stability and successful functionalization. As shown in

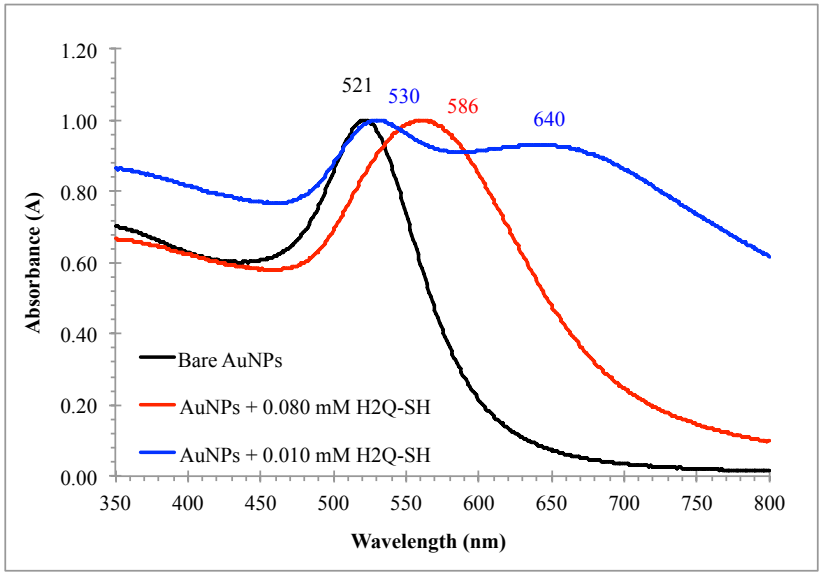

Figure 13: UV-vis spectra of AuNPs functionalized with H_2Q-SH by direct exposure.

Figure 13, the absorption peak for AuNPs functionalized directly with H_2Q-SH shifts by at least 9 nm to longer wavelengths. The UV-vis spectrum for AuNPs functionalized with 0.010 mM H_2Q-SH suggests two populations of nanoparticles: one with an absorption maximum at 530 nm, and the other with an absorption maximum at 640 nm. In addition, the absorption bands for both populations of AuNPs broadened significantly, and the absorption increased at longer wavelengths. Combined with visual observations, these results indicate significant particle aggregation.

To improve stability, AuNPs were functionalized with SPPP, an electrostatic stabilizing agent. A place-exchange reaction was then performed to functionalize AuNPs with H_2Q-SH. As shown in Figure 14, AuNPs functionalized with 0.080 mM H_2Q-SH are very unstable, as indicated by a red-shift of 69 nm accompanied by significant peak broadening. Instability is attributed to the general insolubility of H_2Q-SH in water. Upon adsorption, H_2Q-SH imparts this insolubility

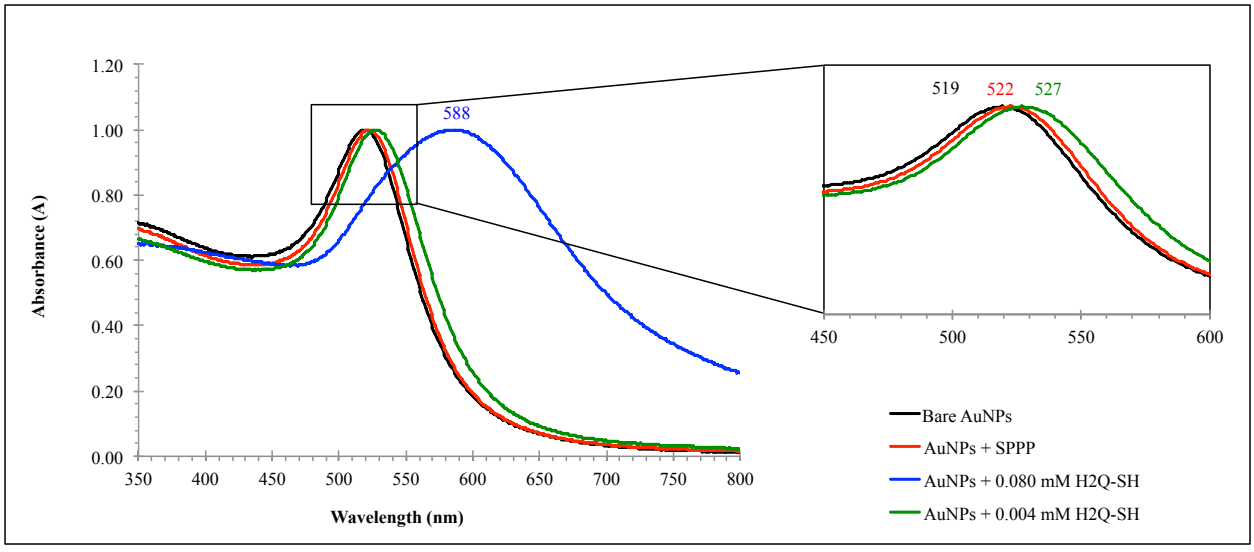

Figure 14: UV-vis spectra of AuNPs functionalized with H_2Q-SH following a place-exchange reaction with SPPP.

to the AuNPs as a whole, causing complete precipitation. As a result, lower concentrations of H_2Q-SH were used to avoid precipitation. As seen in Figure 14, AuNPs functionalized with 0.004

mM H_2Q-SH show a red-shift of only 7 nm, and the peak shape is largely retained. This suggests successful functionalization with H_2Q-SH without sacrificing particle stability.

Cyclic voltammetry was performed to assess the electrochemical activity of these AuNPs. As discussed in section 1.2, cyclic voltammetry is an electrochemical technique in which current (reaction rate) is measured as a function of applied potential (driving force for the reaction). Figure 15 shows the potential sweep technique used for cyclic voltammetry. The potential is scanned over a range that encompasses the standard reduction potential for the molecule of interest, crossing E^o in each direction. **Figure 16** shows typical voltammograms for free H_2Q in solution and for a H_2Q-SH monolayer on the surface of the gold electrode. In this case, the potential is scanned

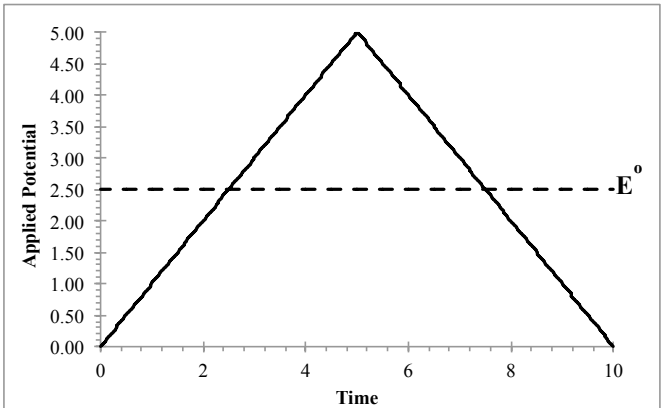

Figure 15: Potential sweep method for cyclic voltammetry.

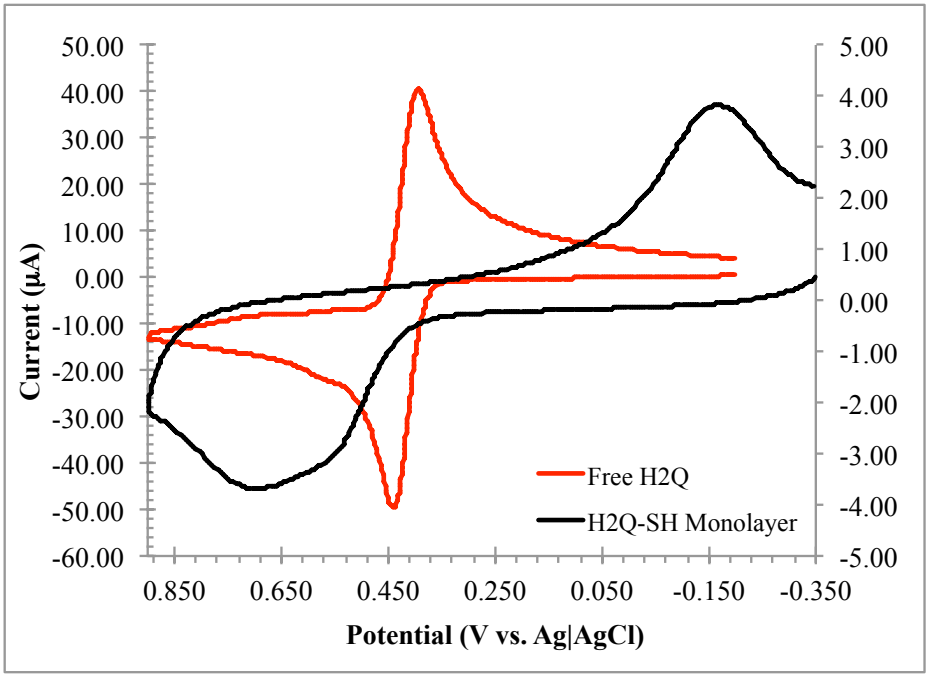

Figure 16: Cyclic voltammograms of 1 mM H_2Q and of a H_2Q-SH monolayer on the surface of a gold electrode. The supporting electrolyte was 0.1 M H_2SO_4, and the scan rate was 100 mV/s.

from -350 mV to 900 mV, and then back to -350 mV. As the applied potential approaches the standard reduction potential of free H_2Q, a peak in oxidative (negative) current is observed. As the potential is scanned to more positive potentials, however, the current decays because it is limited by diffusion. H_2Q must diffuse from bulk solution to the electrode surface, which limits the rate of the reaction, or the amount of current that flows. The same current peak and subsequent decay is observed for the cathodic (positive) current. Increased peak separation is observed for the H_2Q-SH monolayer because electrons must tunnel down the length of the alkanethiol chain to induce a redox reaction.[24]

The redox behavior of electrochemically active AuNPs is expected to be similar to free H_2Q in solution.[29] In fact, because of some unavoidable adsorption to the electrode surface, the difference between cathodic and anodic peak potentials is often lower than the 59 mV value expected for a reversible, single-electron wave.[29] Figure 17 shows the cyclic voltammogram for

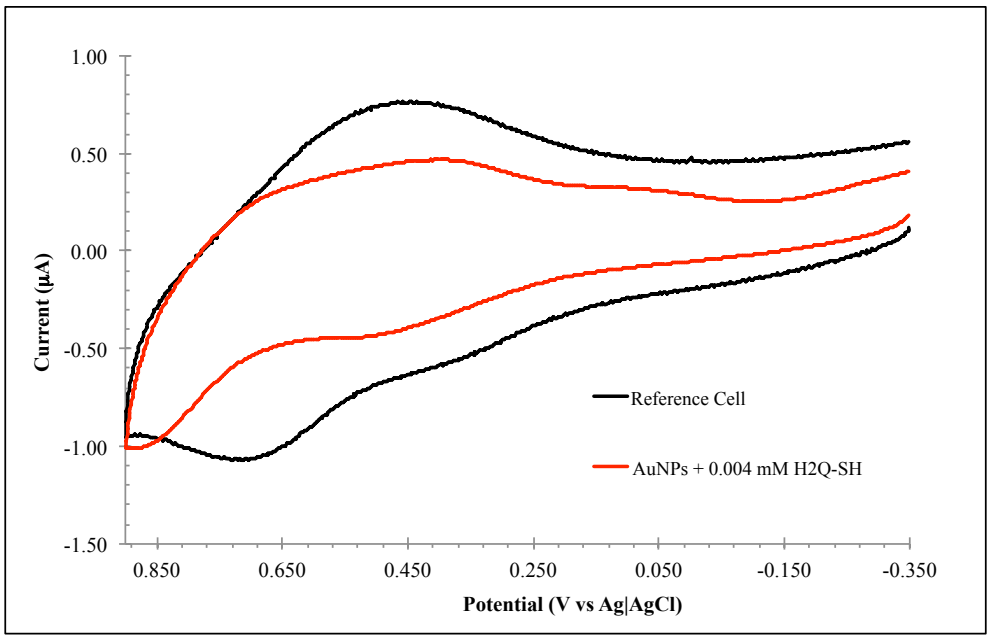

Figure 17: Cyclic voltammogram of AuNPs functionalized with 0.004 mM H_2Q-SH using a place-exchange method with SPPP. The supporting electrolyte was 0.1 M H_2SO_4, the working electrode was a gold microelectrode, and the scan rate was 100 mV/s. Reference cell contains only the supporting electrolyte.

AuNPs functionalized with 0.004 mM H_2Q-SH using the place-exchange reaction with SPPP. These AuNPs do not display any electrochemical activity compared to a reference cell. Cyclic voltammetry is capable of detecting the electrochemical activity of AuNPs in which there are only 7 redox-active molecules per individual nanoparticle.[29] This corresponds to a total concentration of approximately 200 μM. Using Leff's method, the number of gold atoms per nanoparticle can be calculated, as shown in equation *(2)*.[45] *D* is the diameter of the AuNP and v_g is the volume of a single gold atom, estimated to be 17 Å^3.

$$N_{Au} = \frac{4\pi\left(\frac{D}{2}\right)^3}{3v_g} = \frac{4\pi\left(\frac{2}{2}\right)^3}{51} = 269\ atoms/particle \qquad (2)$$

Using this value, it is possible to calculate the mass of a single particle, as shown below.

$$269\ \frac{atoms}{particle} \times \frac{1}{6.02\times10^{23}\frac{atoms}{mol}} \times 196.96\frac{g}{mol} = 8.801\times10^{-20}\frac{g}{particle}$$

Researchers used 200 mg of AuNPs, which they estimate was approximately 75% gold. Therefore, the total mass of all AuNPs was approximately 160.5 mg. From this information, we can calculate the total number of redox active molecules in 100 mL of solution, as shown below.

$$\frac{160.5\ mg}{8.801\times10^{-17}\frac{mg}{particle}} = 1.823\times10^{18}\ particles \times 7\frac{atoms}{particle} \times \frac{1}{6.02\times10^{23}\frac{atoms}{mol}} = 2.12\times10^{-5} mol$$

$$\frac{2.12\times10^{-5}\ mol}{0.100\ L} = 212\ \mu M$$

Therefore, approximately 200 μM H_2Q-SH is required for electrochemical detection. In order to achieve sufficient coverage, a more efficient way of depositing H_2Q-SH must be explored.

Functionalizing AuNPs with hydrophilic mercaptoalkanes, as opposed to electrostatic stabilizers, has been shown to preserve the colloidal suspension and enhance stability.[10,39,43] Increased stability stems from both entropic and osmotic considerations. Molecules in the SAM have greater freedom when the particles are dispersed in solution. As two nanoparticles approach

each other, interpenetration of the monolayers results in a more ordered structure, which is entropically disfavored. Furthermore, this interpenetration process would force water away from the SAM surface. By depleting the SAM interface of water, an osmotic pressure gradient is established that counteracts aggregation. Thus, functionalizing the particles with alkanethiol ligands prevents aggregation through both entropic and osmotic factors.[46]

To improve the stability of AuNPs functionalized with H_2Q-SH, thioctic acid (TA) was used a stabilizing agent. The structure of TA is shown in Figure 18. The terminal carboxylic acid moiety, deprotonated under typical solution conditions, has been shown to improve AuNP stability through electrostatic repulsion and greater hydration of the functional group.[43] In addition TA was previously used to stabilize AuNPs for further functionalization with positive, negative, and neutral moieties.[39]

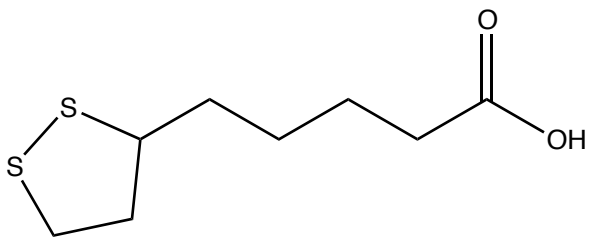

Figure 18: Molecular structure of thioctic acid (TA).

To create mixed monolayers of TA and H_2Q-SH, a place-exchange reaction was performed in which AuNPs were initially functionalized with thioctic acid (TA). Because there is always an equilibrium between bound and unbound molecules in a SAM, subsequent exposure to H_2Q-SH results in the exchange of TA for H_2Q-SH.[9,20,47] AuNPs were prepared as described in section 2.3.1, and the results are summarized in Table 1. In addition to UV-vis, AuNPs were characterized by dynamic light scattering (DLS). DLS gives the hydrodynamic diameter of particles in solution. Successful functionalization with TA should increase the hydrodynamic diameter by twice the length of the TA moiety. Using a length of 0.13 nm per methylene group (along the molecular axis) and a length of 0.18 nm for a carbon-sulfur bond length, a fully extended TA

molecule is approximately 1 nm in length. Thus, the hydrodynamic diameter should increase by approximately 2 nm upon functionalization. DLS measurements also give the polydispersity index (PDI) for particles in solution. The PDI, which varies between 0 and 1, reflects particle size distribution. Smaller values indicate greater size uniformity.

Volume of 1.0 M NaOH (μL)	[TA] (mM)	$\Delta\lambda_{max}$	Hydrodynamic Diameter (nm)	PDI
20.00	1.000	1	13.4	0.97
	0.100	0	11.7	0.57
	0.010	0	12.2	0.86
	0.001	0	48.8	0.57
10.00	1.000	3	12.7	0.44
	0.100	3	11.6	0.49
	0.010	0	13.0	0.51
	0.001	0	10.6	0.53
5.00	1.000	8	11.5	0.40
	0.100	5	8.7	0.57
	0.010	3	22.5	0.57
	0.001	NA	NA	NA

Table 1: AuNPs functionalized with TA at various pH values and ligand concentrations.

As shown in Table 1, the procedure for TA functionalization was optimized for pH and concentration of TA. Basic conditions were needed to ensure that all carboxylic acid moieties were deprotonated. The pKa of free TA is 4.8.[48] However, immobilizing TA on the surface of a nanoparticle increases its pKa because of electrostatic repulsion between neighboring TA molecules. Electrostatic repulsion becomes more significant as the size of the AuNP increases, and the pKa has been shown to reach values near 8 for 7 nm AuNPs.[49] Therefore, more basic conditions are required to reach complete deprotonation. If the pH is not high enough, as with the 5 μL NaOH studies, large shifts in the UV-vis spectra are observed. As shown in Figure 19, the peak broadened significantly for the 1 mM TA sample. In addition, the hydrodynamic diameter

showed great variation, ranging from 8 to 22 nm. Combined, these two results indicate that AuNPs were not stable in solution, most likely because sufficient deprotonation did not occur.

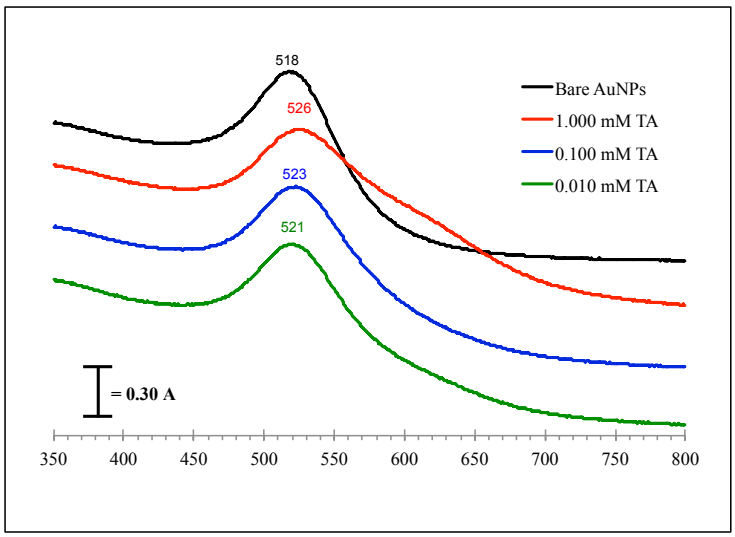

Figure 19: UV-vis spectra for AuNPs functionalized with TA using 5 μL NaOH.

There is also a tradeoff in stability between pH and ionic strength. Increasing the pH ensured complete deprotonation but simultaneously increased the ionic strength of the solution. High ionic strength decreases particle stability by screening the electrostatic repulsion between particles. This effect is observed for AuNPs functionalized with TA using 20 μL NaOH. Although a 3 nm increase in the hydrodynamic diameter is observed (bare AuNPs had a hydrodynamic diameter of 10.32), the high PDI value suggests significant variation in particle size. In addition, Figure 20 demonstrates that significant peak broadening that occurred for the 0.001 mM TA sample. Combined, these results suggest that 20 μL is also not ideal for particle functionalization, and we attribute this lack of stability to the high ionic strength in solution. Although entropic and osmotic factors also contribute to particle stability, these factors might be less significant because of the structure of TA. We expect the disulfide foot to restrict the

conformational freedom of the alkane chain compared to an alkanethiol with only one bond to the AuNP. Therefore, entropic contributions to stability might be compromised.

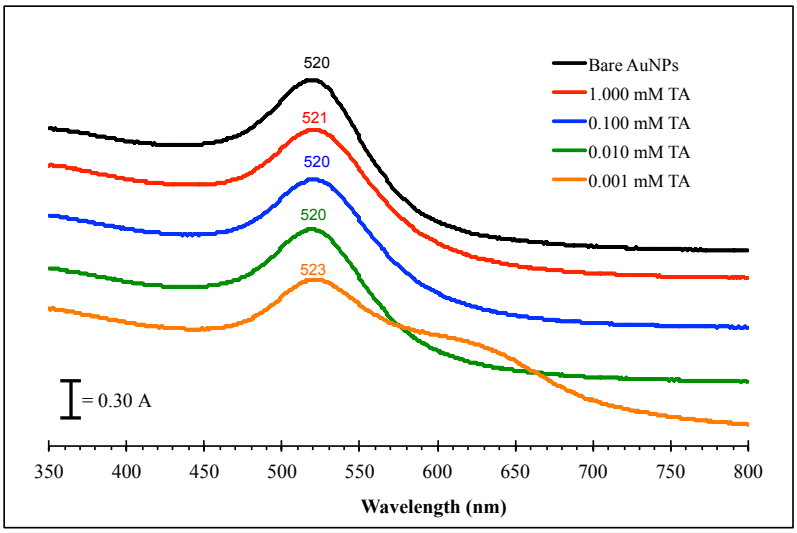

Figure 20: UV-vis spectra of AuNPs functionalized with TA using 20 μL NaOH.

The best results were obtained for particles functionalized with TA using 10 μL NaOH. As seen in Figure 21, red-shifts of 3 nm were observed in the UV-vis spectra, and no significant peak broadening is observed. The hydrodynamic diameter of these particles increases by approximately 2 nm (bare AuNPs possessed a hydrodynamic diameter of 10.00 nm) when TA concentrations above 0.010 mM are used. When the concentration of TA drops below 0.010 mM, the hydrodynamic diameter shows negligible change, and the PDI begins to increase. These data indicate that higher concentrations of TA are needed for successful functionalization. This result is consistent with previous work demonstrating that 0.010 mM is the lowest concentration required to achieve a stable monolayer.[1] In our case, the most stable particles required 1 mM or 0.100 mM TA for functionalization.

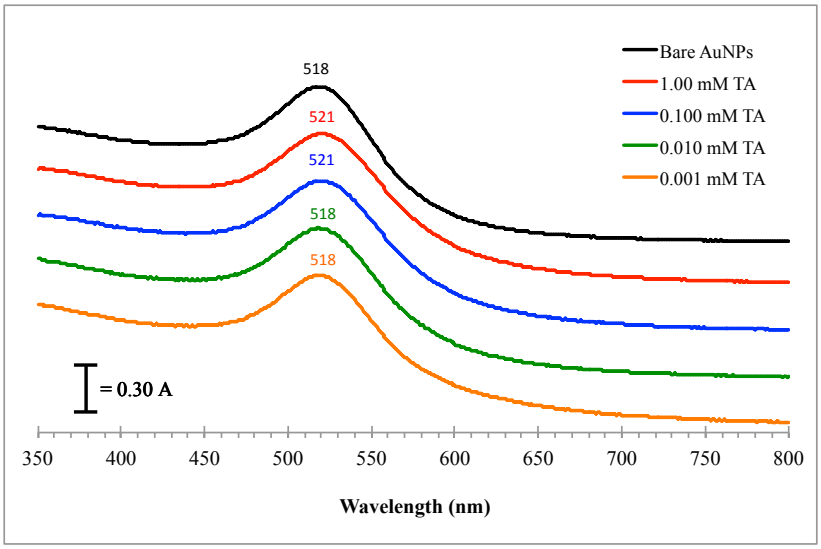

Figure 21: UV-vis spectra of AuNPs functionalized with TA using 10 mL NaOH.

Using this optimized procedure, a place-exchange reaction was performed to functionalize AuNPs with H_2Q-SH. AuNPs functionalized with TA were prepared in solution with various concentrations of H_2Q-SH. Again, the resulting particles were characterized using UV-vis spectroscopy and DLS. The results are summarized in Table 2. With the exception of 1.000 mM TA exchanged by 0.100 mM H_2Q-SH, all show red shifts in their absorbance maxima, suggesting that the place-exchange reaction was successful. The corresponding UV-vis spectra are shown in Figure 22. Minimal peak broadening is observed, and low PDIs confirm that stability is preserved upon functionalization.

[TA] (mM)	[H2Q-SH] (mM)	$\Delta\lambda_{max}$ (from TA)	$\Delta\lambda_{max}$ (total)	Hydrodynamic Diameter (nm)	PDI
1.000	1.000	2	5	15.96	0.483
1.000	0.100	0	3	11.61	0.413
0.100	0.100	2	5	11.37	0.391
0.100	0.001	2	4	11.99	0.507

Table 2: Functionalization of AuNPs with H_2Q-SH using a place-exchange reaction.

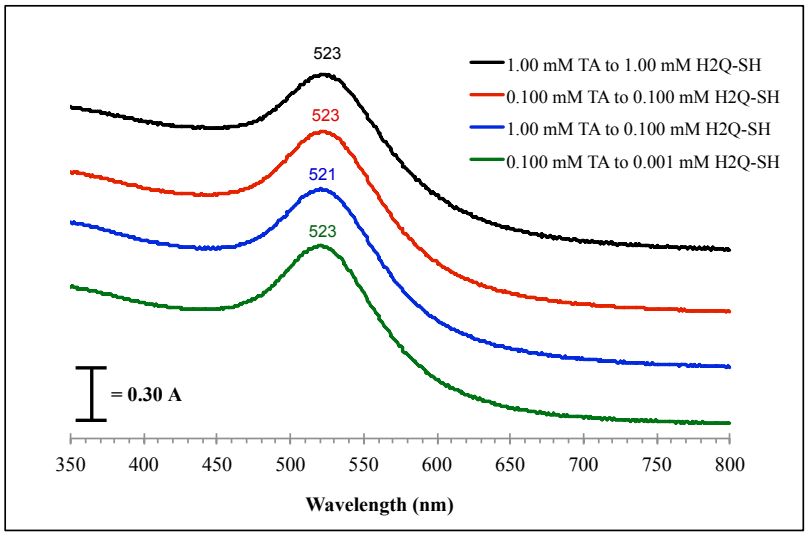

Figure 22: UV-vis spectra of AuNPs functionalized with H_2Q-SH using a place-exchange reaction.

The electrochemical activity of the resulting particles was then assessed using cyclic voltammetry. Unfortunately, cyclic voltammetry of the functionalized particles shows no appreciable redox behavior compared to a reference cell. As shown in Figure 23, the voltammograms are flat, with no discernable peaks corresponding to H_2Q oxidation or reduction. Clearly, the place-exchange reaction fails to deposit sufficient H_2Q-SH for detection by electrochemical means.

To this end, AuNPs were functionalized with H_2Q-SH using a codeposition reaction. Instead of exchanging bound TA with H_2Q-SH, AuNPs were exposed to various concentrations of both alkanethiol moieties. Several trials were attempted in order to achieve a balance between the amount of TA needed for stabilization and the amount of H_2Q-SH needed for electrochemical activity. The composition of the mixed monolayer rarely mirrors that of the solution; however, the two are related in that increasing the mole fraction of one species in solution results in greater

relative deposition of that species. To promote the deposition of H_2Q-SH, the concentration of TA was kept low (either 0.100 mM or 0.050 mM).

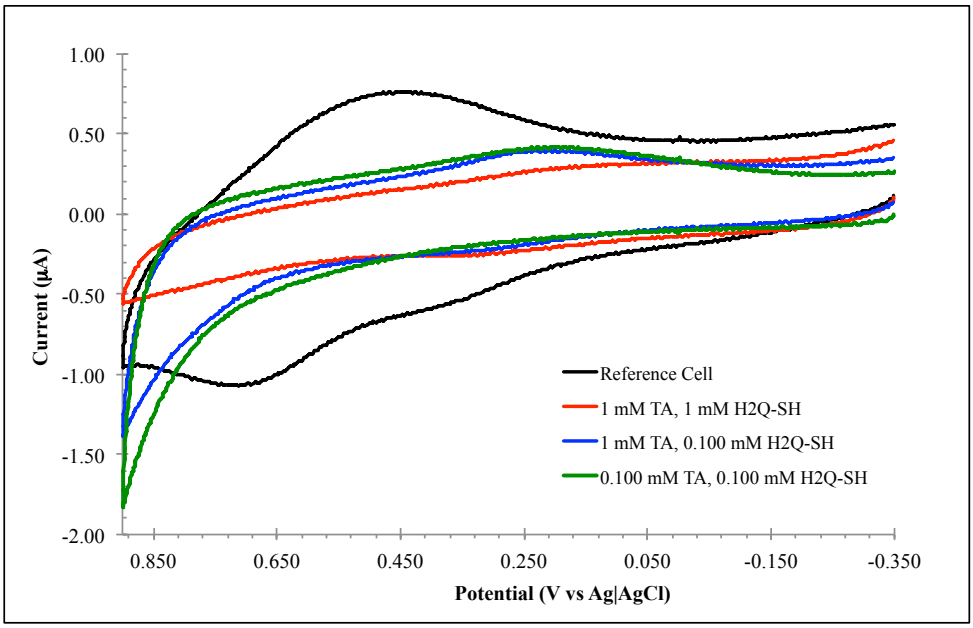

Figure 23: Cyclic voltammograms of AuNPs + H_2Q-SH using a place-exchange reaction. The supporting electrolyte is 10 mM KCl. All scan rates are 250 mV/s.

[TA] (mM)	[H_2Q-SH] (mM)	$\Delta\lambda_{max}$	Hydrodynamic Diameter (nm)	PDI
0.100	0.1000	9	12.63	0.410
	0.0100	2	11.77	0.454
	0.0010	2	11.68	0.561
0.050	0.1000	10	26.99	0.287
	0.0100	4	13.59	0.318
	0.0010	1	13.47	0.535

Table 3: UV-vis and DLS data for AuNPs functionalized with TA and H_2Q-SH using a codeposition method.

Table 3 summarizes DLS and UV-vis data for all codeposition samples. For both sets of codeposition samples (those made with 0.100 mM TA and those made with 0.050 mM TA), larger red-shifts in the UV-vis spectra are observed as the amount of H_2Q-SH in solution increases. DLS data are consistent with these results, as the hydrodynamic diameter of the

particles increases with increasing H_2Q-SH concentration. As seen in Figure 24, UV-vis shifts are also accompanied by significant peak broadening compared to bare AuNPs. This effect is more pronounced when the concentration of TA is decreased to 0.050 M (Figure 24B). The hydrodynamic diameter of particles is also larger at 0.050 mM TA. Combined, these results suggest that, as predicted, more H_2Q-SH is incorporated into the monolayer as the concentration of H_2Q-SH increases relative to TA. However, particle stability is also compromised in these samples.

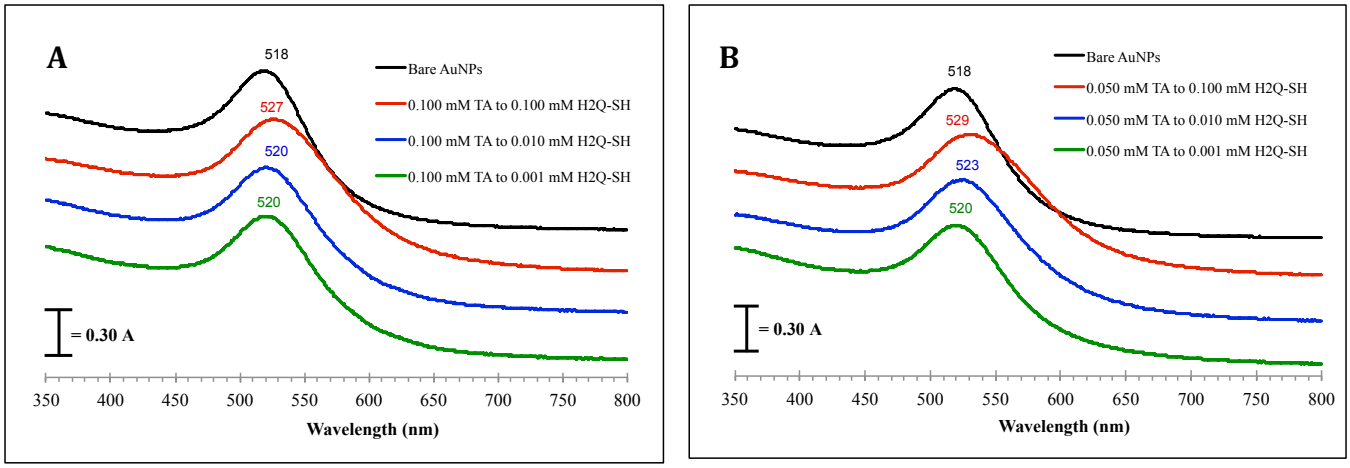

Figure 24: UV-vis spectra of AuNPs functionalized with H_2Q-SH using a codeposition reaction. (A) With 0.100 mM TA (B) with 0.050 mM TA.

Despite decreased stability at higher concentrations of H_2Q-SH, cyclic voltammetry was performed on all samples to assess their electrochemical activity. Unfortunately, none of the samples display significant electrochemical activity compared to a clean reference cell, as shown in Figure 26. Under conditions that produce stable particles in solution, codeposition does not allow sufficient deposition of the H_2Q-SH moiety to produce electrochemically active particles.

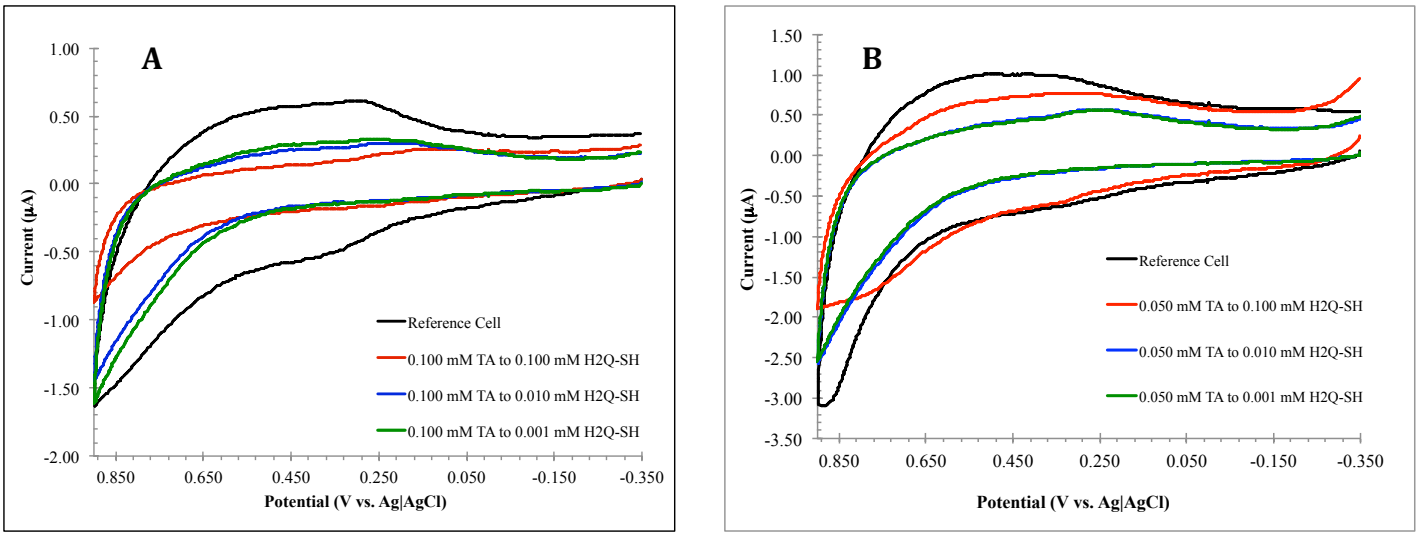

Figure 26: Cylic voltammograms of AuNPs functionalized with (A) 0.100 mM TA or (B) 0.050 mM TA and various concentrations of H_2Q-SH using a codeposition method.

The place-exchange and codeposition studies demonstrated that we could not simultaneously achieve particle stability and sufficient H_2Q deposition in aqueous solution. As a result, ethanol was explored as an alternative solvent system for functionalization. AuNPs were transferred from water to ethanol as described in section 2.4. Once in ethanol, AuNPs were functionalized with H_2Q-SH. UV-vis spectra for the transfer and functionalization process are shown in Figure 25. In agreement with literature, the absorption maximum remains the same upon transfer into ethanol.[40] After functionalization, it shifts to longer wavelengths by 10 nm,

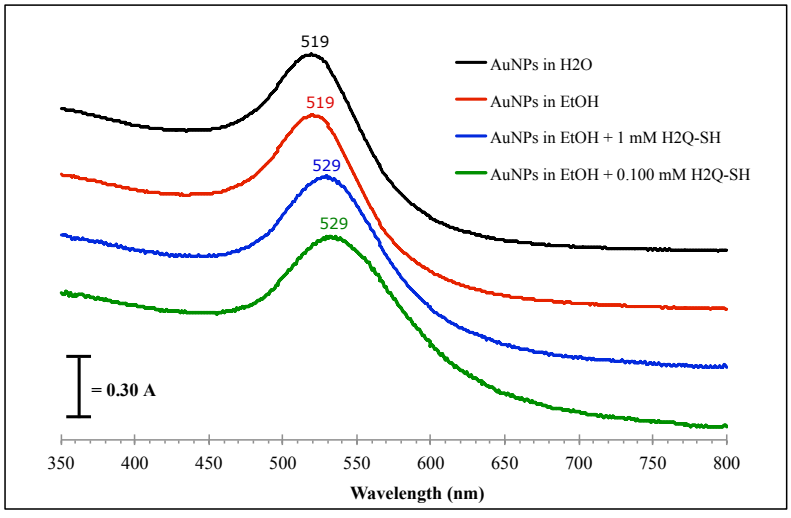

Figure 25: UV-vis spectra of AuNPs functionalized with H_2Q-SH in EtOH.

confirming functionalization with H_2Q-SH. AuNPs functionalized with 0.100 mM H_2Q-SH ultimately precipitated from solution. AuNPs functionalized with 1.000 mM H_2Q-SH remained stable indefinitely.

Therefore, cyclic voltammetry was performed on this sample to assess the electrochemical activity of the functionalized particles. As seen in Figure 27, significant redox activity is observed in these samples. Distinct oxidation and reduction peaks are observed with peak separation between that of free hydroquinone and the H_2Q-SH monolayer. However, quantitative analysis of this sample is hindered by AuNP adsorption to the electrode surface. After rinsing the electrode and returning it to a clean reference cell, nearly the same redox behavior is observed, as shown in Figure 28. As a result, only tentative conclusions can be drawn about the creation of

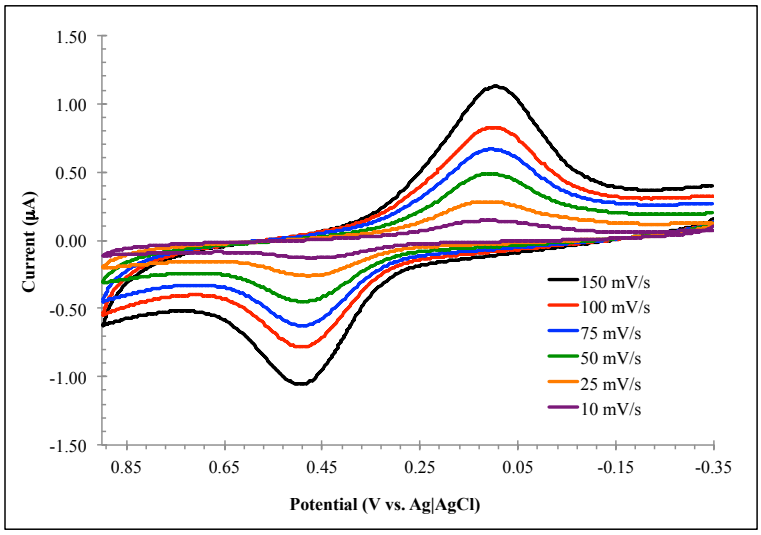

Figure 27: Cyclic voltammograms of AuNPs functionalized with 1.000 mM H_2Q-SH in EtOH. The supporting electrolyte was 0.100 M H_2SO_4.

electrochemically active AuNPs. In an attempt to prevent adsorption, AuNPs were functionalized with SPPP, an electrostatic stabilizing agent possessing a net negative charge, before functionalization with H_2Q-SH. Although a few AuNPs might still stick to the electrode surface, further AuNP adsorption is discouraged by electrostatic repulsion. However, SPPP

functionalized AuNPs proved to be unstable in ethanol and precipitated after a few hours. As a result, current work involves finding an electrode that will prevent AuNP adsorption or modifying the gold electrode for more quantitative analysis.

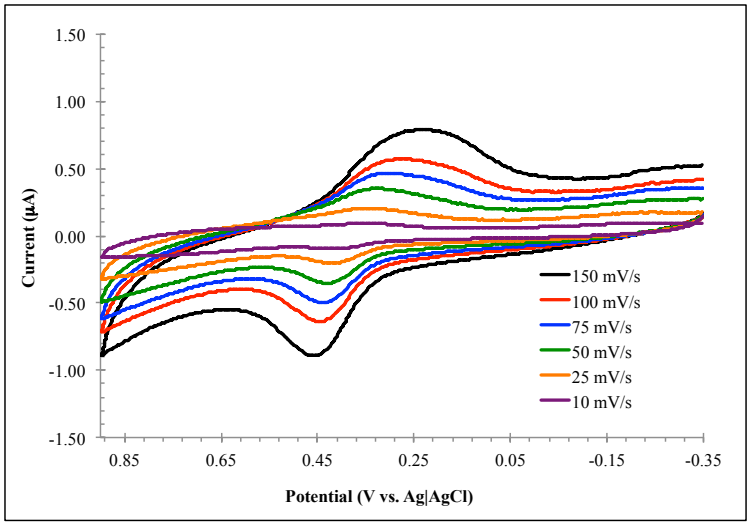

Figure 28: Cyclic voltammograms of Au electrode in a clean reference cell after soaking in AuNP sample.

3.2 Electrochemically Active Polystyrene Spheres

To avoid the instability of AuNPs, PS-NH_2s were used to create electrochemically active particles. PS-NH_2s possess a high density of amine functional groups on their surface. These amine groups electrostatically stabilize the particles, improving their stability in solution. Sulfo-SMCC, an amine-thiol crosslinker, was used to couple PS-NH_2s to H_2Q-SH. Alternatively, EDC and sulfo-NHS, reagents for amine-carboxy coupling, were used to link PS-NH_2s to DHB, a hydroquinone species possessing a carboxylic acid functional group. Before any coupling was attempted, however, it was necessary to establish that PS-NH_2s did not interfere with H_2Q or DHB redox chemistry. As seen in Figure 29, the redox activity for free H_2Q remains largely unchanged upon the addition of PS-NH_2. As seen in Figure 30, however, the presence of PS-NH_2 has a marked effect on the redox behavior of free DHB. The overall current is significantly

reduced, and the peak separation dramatically increases. Nevertheless, the presence of PS-NH_2 does not prevent the electrochemical detection of either of free DHB or free H_2Q.

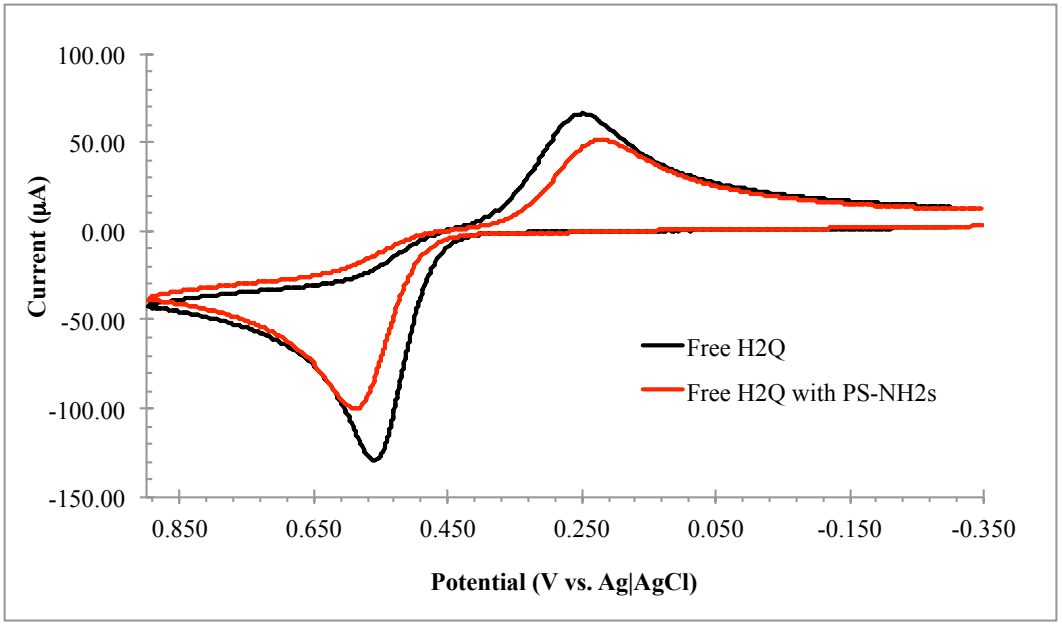

Figure 29: Cyclic voltammograms for free H_2Q and free H_2Q with PS-NH_2s. The supporting electrolyte was 0.1 M H_2SO_4 and the working electrode was a GCE.

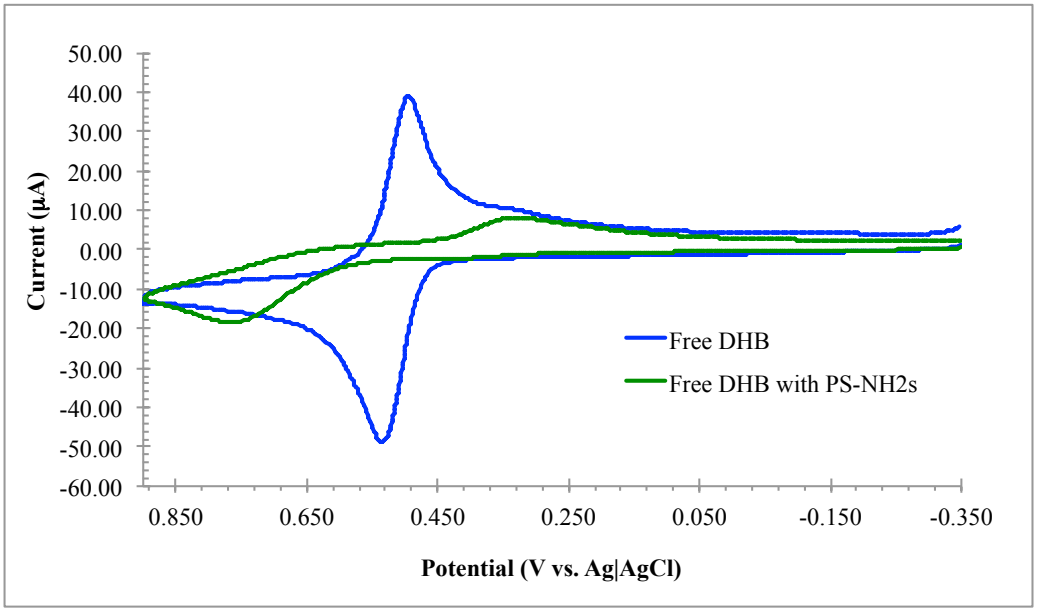

Figure 30: Cyclic voltammograms for free DHB and free DHB with PS-NH_2s. The supporting electrolyte was 0.1 M H_2SO_4 and the working electrode was a gold microelectrode.

With these control studies completed, amine-thiol coupling was attempted using sulfo-SMCC. PS-NH_2s were linked to either MHA or carboxy-PEG to test the coupling procedure. The results of these coupling attempts, as well as initial values for the hydrodynamic diameter of both particle types, are summarized in Table 4. Higher concentrations of sulfo-SMCC greatly de-stabilized the particles, as evidenced by hydrodynamic diameters above 1000 nm. When 2 mM sulfo-SMCC is used to couple PS-NH_2s to MHA, a large increase in the hydrodynamic diameter is observed, as well. MHA should only increase the hydrodynamic diameter by approximately 2 nm. Therefore, the dramatic increase from 253.6 nm to 399.7 nm is much larger than we would expect. A 50 nm increase in the hydrodynamic diameter was observed when 2 mM sulfo-SMCC was used to couple PS-NH_2s to carboxy-PEG. This increase is also larger than expected based on

PS-NH_2 Source	[sSMCC] (μM)	Coupled to 500 μM:	Hydrodynamic diameter (nm)
Bang's Labs	none	none	253.6
	200.00	MHA	1537
	200.00	PEG	1352
	2.00	MHA	399.7
	2.00	PEG	312.5
Magsphere	none	none	214.9
	none	PEG	2338
	none	MHA	4203
	2.00	PEG	209.6 (76.3%) 1319 (23.6%)
	2.00	MHA	2984

Table 4: Summary of amine-thiol coiupling attempts using sulfo-SMCC. 10% PS-NH_2 was used for all trials.

literature values for AuNPs functionalized with PEG. Liu and coworkers reported an increase in the hydrodynamic diameter of 9.5 nm after functionalizing AuNPs with 1500 MW PEG and 18.2 nm after functionalization with 5000 MW PEG.[50] Since our carboxy-PEG has a MW of 2400 Da,

we expect the hydrodynamic diameter to increase in the range of 9.5 to 18.2 Da. Therefore, an increase of 50 nm indicates significant particle instability.

Furthermore, this result was not reproducible using a new source of PS-NH_2 (Magsphere). The identical coupling procedure resulted in hydrodynamic diameters greater than 1000 nm. Given the universal lack of stability observed with these samples, a modified procedure was attempted in which a few drops of DMF were added to the solution during coupling. Small amounts of DMF are commonly used to improve particle stability during coupling. The results from these coupling attempts are shown in Table 5. Unfortunately, the presence of DMF failed to increase stability. In fact, the hydrodynamic diameter increased compared to the coupling procedure without DMF. Therefore, adding DMF failed to improve particle stability in this coupling procedure.

[sSMCC] μM	Coupled to 500 μM	Hydrodynamic diameter (nm)
2	PEG	4498
2	MHA	2401

Table 5: Sulfo-SMCC coupling of Magsphere PS-NH_2s to carboxy-PEG or MHA using sulfo-SMCC and a few drops of DMF.

Amine-carboxy coupling was also attempted using EDC and sulfo-NHS. In addition to the concentration of EDC, the volume of PS-NH_2 was also varied. Results are summarized in Table 6. An increase of about 6 nm was observed for 10% PS-NH_2 functionalized with 2 mM EDC, suggesting successful coupling

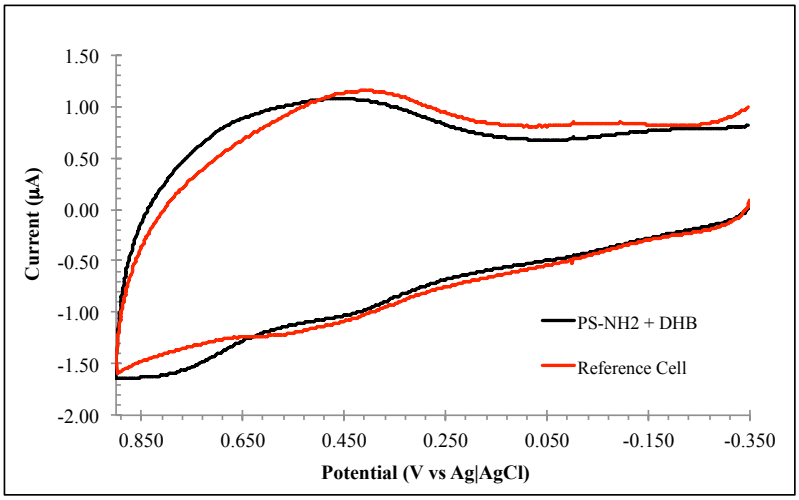

Figure 31: Cyclic voltammogram of PS-NH_2s coupled to DHB. The supporting electrolyte was 0.10 M H_2SO_4 and a gold microelectrode was used as the working electrode.

to DHB. However, as shown in Figure 31, these particles did not possess any electrochemical activity compared to a clean reference cell.

Decreasing the amount of PS-NH_2 decreased particle stability, as evidenced by the hydrodynamic diameter of 3529 nm. Even when the amounts of EDC, sulfo-NHS, and DHB were adjusted accordingly, particle instability persisted. However, this final sample was also prepared using Magsphere PS-NH_2s. As a result, the lack of stability might be attributed to the new particle source. Further trials are needed to optimize coupling for these particles.

% PS-NH_2 (v/v)	[EDC] (mM)	[sulfo-NHS] (μM)	[DHB] (μM)	Hydrodynamic Diameter (nm)
10.00	2.00	5.00	200.00	260.3
1.00	2.00	5.00	200.00	3529
1.00	0.20	0.50	20.00	885.9

Table 6: Summary of amine-carboxy coupling attempts using EDC and sulfo-NHS.

3.2.1 Controls for amine-carboxy PS-NH_2 coupling

Given that no electrochemical activity was observed in the PS-NH_2 samples, it was important to establish whether any coupling had occurred. To this end, several controls were performed to test EDC coupling. The first involved dialysis of a PEG-NH_2 moiety that was coupled to DHB as described in section 2.5.3. The sample was added to dialysis tubing with a molecular weight cutoff of 5300 kDa. PEG-NH_2 (MW 5300 kDa) was too large to pass through the membrane. Therefore, uncoupled DHB would diffuse away, while DHB coupled to PEG-NH_2 would remain inside the dialysis tubing. Using cyclic voltammetry, the electrochemical activity of both the inner and outer membrane solutions was monitored to determine if successful coupling occurred. Figure 32 shows the results from this experiment. Electrochemical activity was observed in aliquot 1, the first sample taken from the outer solution. This electrochemical

activity undoubtedly corresponds to excess DHB that diffused from inside the dialysis tubing. Essentially no electrochemical activity is observed in aliquot 2, the second sample removed after the outer solution was refreshed and re-equilibrated. This indicates that excess DHB is successfully removed from the inner-membrane solution. No electrochemical activity is observed for the PEG-NH_2 sample. Either coupling was unsuccessful, or coupling resulted in a DHB species that is no longer electrochemically active.

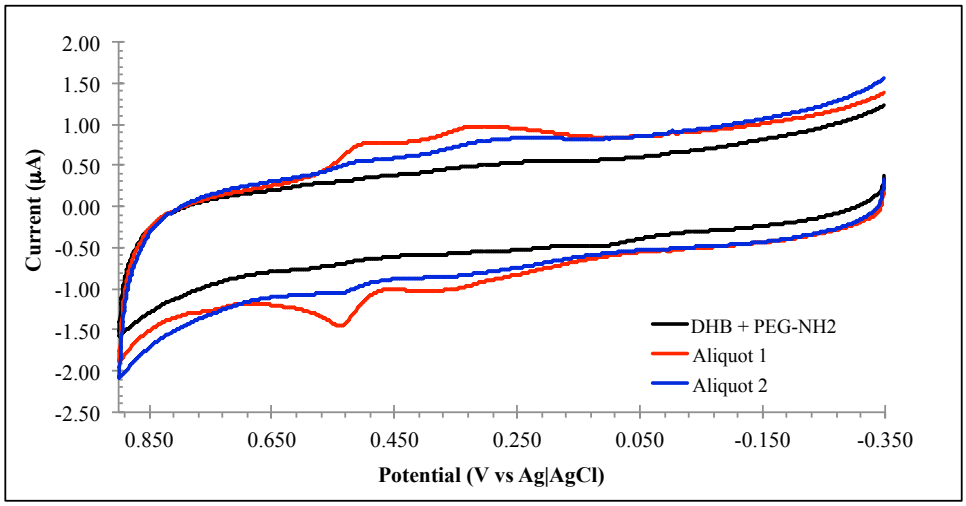

Figure 32: Cyclic voltammograms for dialysis tubing samples to test EDC/sulfo-NHS coupling.

To further assess the success of coupling, PS-NH_2s were coupled to the thermoresponsive polymer polyNIPAM, as discussed in section 2.5.3. PolyNIPAM undergoes a phase transition at 35 °C. Below this temperature, polyNIPAM is soluble in water, but above this temperature, it readily precipitates from solution.[51, 52] Therefore, if tethered to the PS-NH_2s, complete precipitation should occur if the temperature is raised above 35 °C. Temperature controlled UV-vis absorption measurements were performed on PS-NH_2s + polyNIPAM, and the results are shown in Figure 33. When the temperature is raised to 45 °C, the polystyrene spheres precipitate from solution, resulting in a decreased absorbance (black dashed line). When the sample is

inverted, the absorbance increases, but does not return to its original value (black dotted line). The same decrease in absorbance is not observed for PS-NH_2s and free polyNIPAM in solution (blue lines), nor for PS-NH_2s alone. This suggests successful coupling of polyNIPAM to the PS-NH_2s.

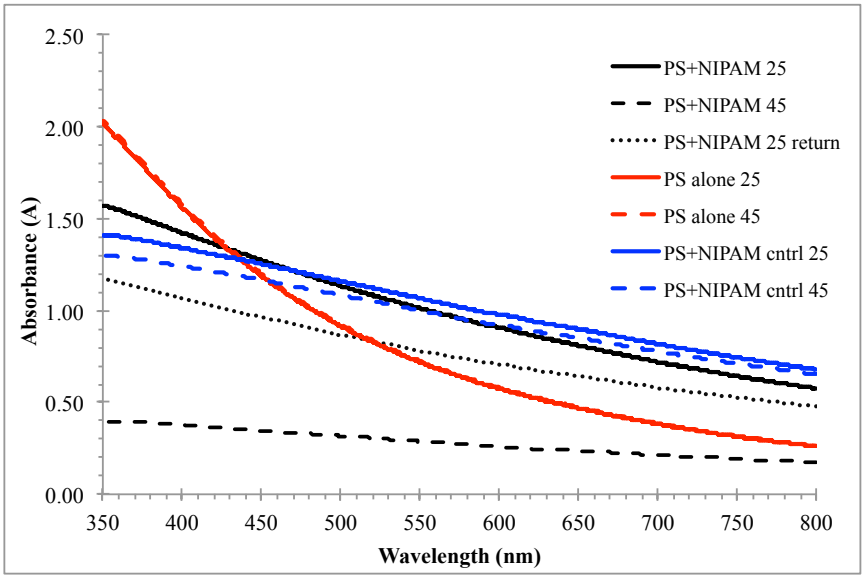

Figure 33: Temperature controlled UV-vis studies of PS-NH_2 + polyNIPAM.

3.3 Electrochemically active mixed monolayers

Electroactive mixed monolayers were also examined on planar substrates. A fundamental understanding of nanoscale charge transfer is essential for many life processes, and SAMs are an easy way to study this. In order to examine differences in electron tunneling pathways, three different electrochemically active mixed monolayers were studied. As discussed in section 1.3.3, these monolayers were composed of electroactive H_2Q-SH along with inert alkanethiol spacers of varying chain length. These alkanethiol spacers included hexanethiol (HT), octanethiol (OT), and dodecanethiol (DT). Mixed monolayers were assembled by forming a pure monolayer of the inert alkanethiol. A place-exchange reaction was then performed to exchange some of the inert

alkanethiol with H_2Q-SH. The composition of these mixed monolayers was studied as a function of time using cyclic voltammetry and chronoamperometry.

As discussed in section 2.8.2, chronoamperometry is a potential step technique in which current decay is recorded as a function of time. Figure 34 shows a typical chronoamperogram. The observed current can be broken down into faradaic and non-faradaic components. Faradaic current results from the redox reactions of electroactive molecules. Non-faradaic current results from charging the electrical double layer. The movement of ions to and from the electrode surface registers as current. To determine the quantity of electroactive molecules in the

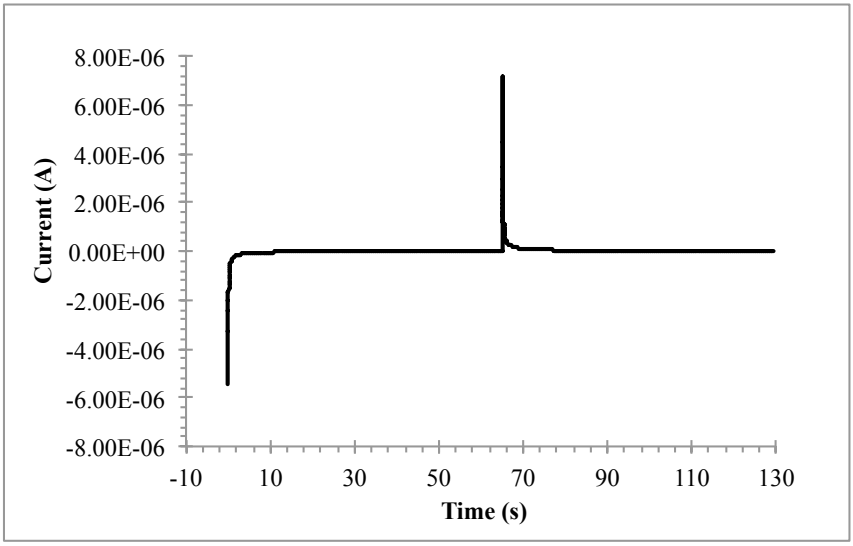

Figure 34: Chronoamperogram of a mixed monolayer of DT and H_2Q-SH on a gold microelectrode. First potential step was 900 mV and second potential step was -350 mV.

monolayer, we are only interested in faradaic current. To limit the contribution from non-faradaic current, current from the inert alkanethiol monolayer was subtracted from all chronoamperograms. Integrating the corrected current decay yields the total amount of charge, which, using Faraday's constant and stoichiometry, can be converted into the total number of electroactive molecules. This value allows us to quantify the composition of various mixed monolayers.

Figure 35 shows the composition of a DT monolayer after place-exchange with H_2Q-SH as a function of time. To account for variations in the electrode surface area, monolayer composition is calculated as a percentage of a pure H_2Q-SH monolayer ($\Gamma QH_2/\Gamma_{max}$). The surface density of H_2Q-SH was calculated to be 2.74×10^{-10} mol/cm^2. The value was of the same order of magnitude as previous literature values reporting a surface density of 5.40×10^{-10} mol/cm^2.[22] The slightly lower surface density can be attributed to a rougher electrode surface, leading to a more disordered monolayer and less efficient packing of molecules. For DT place-exchange, maximum exchange was observed after 72 hours, reaching a value of approximately 14% H_2Q-SH (averaging the steady state values for both cathodic and anodic currents).

To help ensure that all molecules of H_2Q-SH occupied equivalent sites, the monolayer was backfilled with DT. In other words, an additional place-exchange reaction was performed over 24 hours to replace H_2Q-SH occupying defect sites with DT. Because electron transfer in monolayers is mediated by defect sites, this backfilling process is important to ensure that

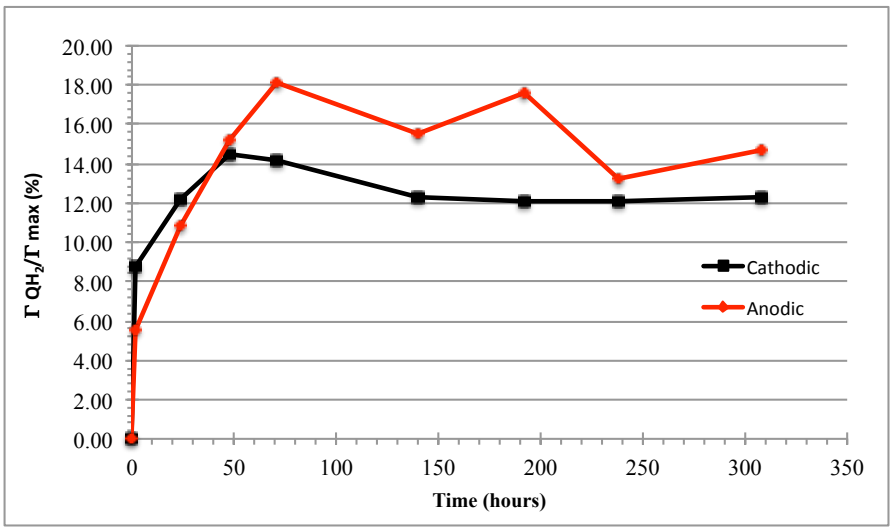

Figure 35: Percent composition of a mixed monolayer containing DT and H_2Q-SH as a function of time for the place-exchange reaction.

electron tunneling down the full length of the monolayer is measured.[20] After backfilling with DT, the composition of H_2Q-SH dropped to 12–14%.

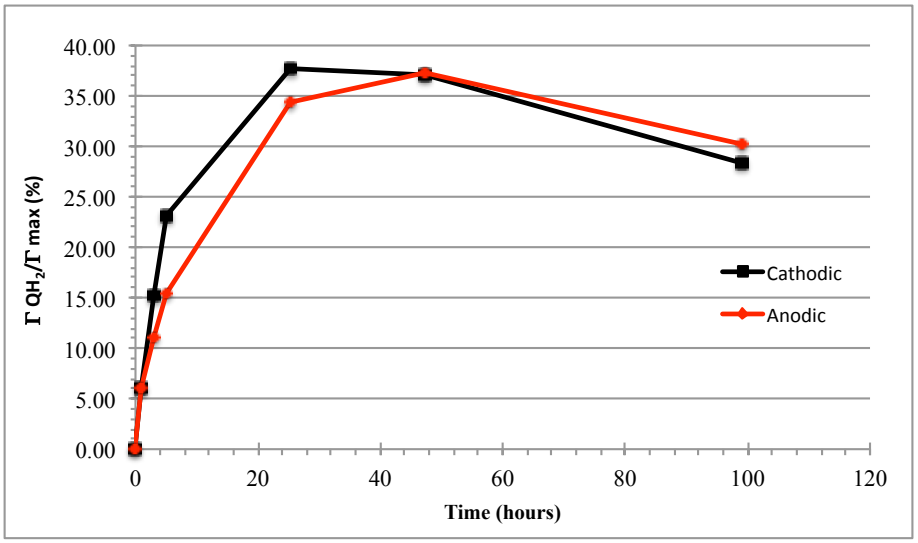

Figure 36: Percent composition of a mixed monolayer of OT and H_2Q-SH as a function of time for a place-exchange reaction.

The same experiment was performed with an OT monolayer, and the results are shown in Figure 36. In this case, maximum exchange occurred after approximately 24 hours, with a H_2Q-SH composition of 34% (again averaging steady state values for cathodic and anodic current). After backfilling, the composition of H_2Q-SH drops to 8–14%.

Finally, the experiment was repeated with a mixed monolayer of HT and H_2Q-SH. As shown in Figure 37, the exchange is much faster and reaches a higher surface density of H_2Q-SH. Ignoring the anodic data, maximum exchange occurs after only 1 hour, with a H_2Q-SH surface density of 42–47%. After backfilling, the H_2Q-SH surface density drops to only 4–5%. Clearly, the H_2Q-SH species are much easier to exchange in the HT mixed monolayer than in the DT or OT mixed monolayers. This can likely be attributed to a high degree of disorder in the HT mixed monolayer compared to the other monolayers, in which stronger van der Waals forces stabilize the monolayer structure. At this point, we are unsure why there is such a great difference

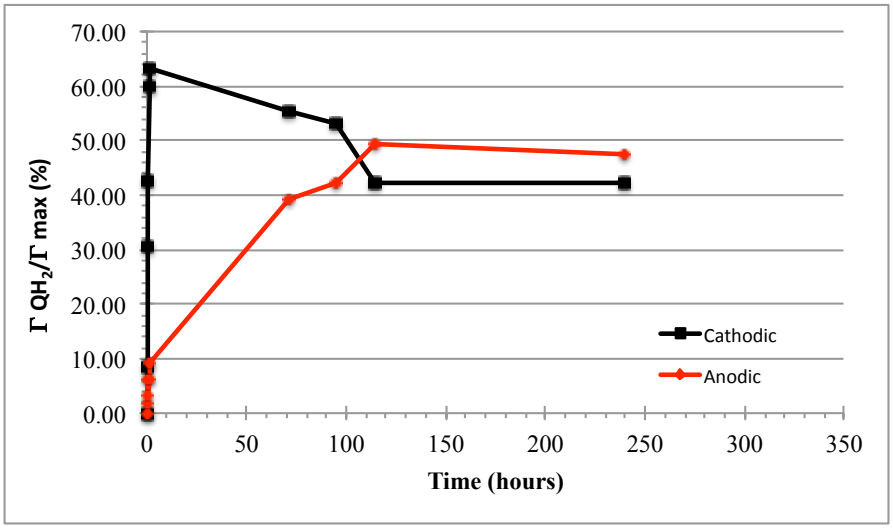

Figure 37: Percent composition of a mixed monolayer of HT and H_2Q-SH as a function of time for the place-exchange reaction.

between the cathodic and anodic current at shorter time scales. Preliminary analyses suggest that determining the total charge from cyclic voltammograms produces better results. Nevertheless, additional trials are necessary to elucidate the origin of this behavior.

The rate of exchange and overall composition of these three monolayers makes sense given the size of the alkanethiols. HT shows the fastest exchange rate because its shorter chain reduces the van der Waals forces between neighboring chains.[9,53] Therefore, desorption occurs more readily. DT shows the slowest exchange rate because its longer chain length makes desorption more difficult. Because OT is intermediate in size between HT and DT, it exchanges faster than DT but slower than HT. The maximum surface density of H_2Q-SH also correlates with chain length. Because DT is the most difficult to exchange, the % composition of H_2Q-SH is the lowest. HT has the highest % composition, and OT lies in the middle. It is rather surprising that the % composition of H_2Q-SH drops to only 4-5% after backfilling in the HT monolayer. Backfilling had the least significant effect on the DT monolayer, followed by OT and HT.

Cyclic voltammetry was used to compare the oxidation and reduction potentials for H_2Q-SH in each mixed monolayer. The peak separation is related to the tunneling distance in the self-assembled monolayer.[24] Therefore, cyclic voltammetry will give insight into the path of electron transfer in these mixed monolayers. Figure 38 shows cyclic voltammograms for mixed monolayers of H_2Q-SH with DT, OT, and HT. Although it is difficult to observe the oxidation and reduction peak potentials for OT and DT, HT clearly has the smallest peak separation. The peaks corresponding to the DT monolayer are very broad. Although some current is observed before the onset of oxidation or reduction for the OT monolayer, the peaks extend past what appear to

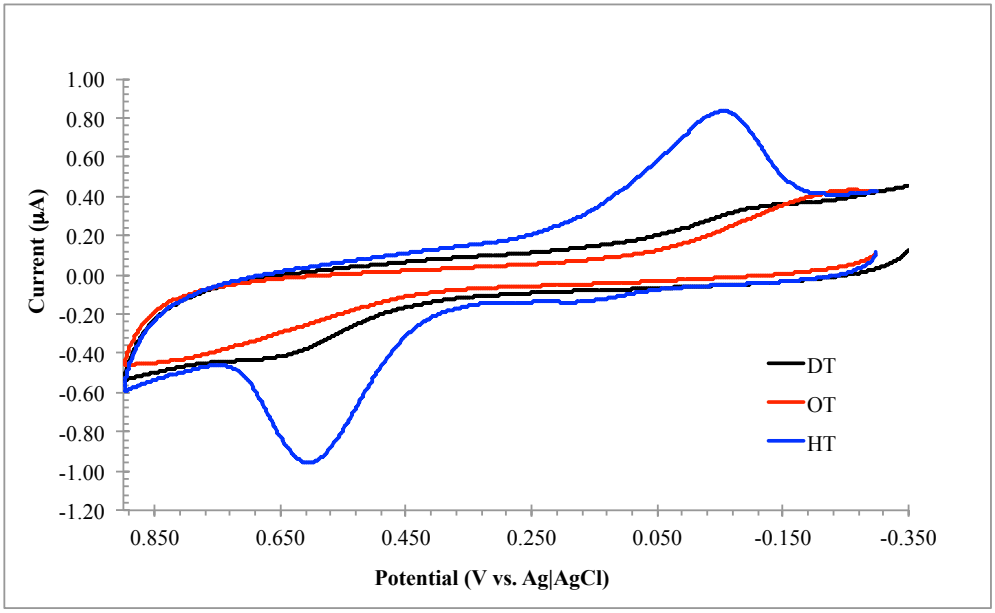

Figure 38: Cyclic voltammograms for mixed monolayers of H_2Q-SH with DT, OT, or HT. The supporting electrolyte was 0.1 M H_2SO_4.

be the maximum peak potentials for the OT monolayer. The potential range for these experiments is limited by gold oxide layer formation at positive potentials and hydrogen gas evolution at negative potentials. Therefore, it is difficult to observe the potential range encompassing the complete voltammogram. Overall, further trials are required to determine the peak potentials for OT and DT monolayers.

4 Conclusion

Several methods for the creation of electrochemically active NPs have been attempted, including place-exchange, codeposition, phase transfer, and organic coupling chemistry with PS-NH_2s. Place-exchange and codeposition methods failed to deposit sufficient H_2Q-SH to be detected by electrochemical means. While phase transfer of AuNPs into ethanol was more promising, significant adsorption of particles to the electrode surface was observed. Therefore, current work involves identifying a working electrode, such as graphene or platinum, which will discourage adsorption. Regarding organic coupling chemistry, further trials are required to optimize the parameters for these reactions. Coupling PS-NH_2s to polyNIPAM provides evidence that coupling occurred, though controls with dialysis tubing did not support this result. Further coupling controls, such as a "reverse" dialysis study, could be performed to confirm coupling. In such a study, free DHB could diffuse into the dialysis sample to couple with PEG-NH_2. Therefore, the extent of coupling could be monitored by a decrease in DHB levels in the outer membrane solution.

Exchange rates and monolayer composition for the DT, OT, and HT mixed monolayers are in accordance with predictions. The DT monolayer showed the slowest exchange and had the lowest percent composition of H_2Q-SH. As the length of the alkanethiol chain decreased, the exchange rate increased, and the percent composition of H_2Q-SH increased. Further trials are necessary to compare the redox potentials for the DT and OT monolayers, as the full range of the voltammograms cannot be observed because of experimental limitations. Additional trials will also be performed using decanethiol (dT) as the inert alkanethiol spacer. Finally, codeposition studies with DT, dT, OT, and HT will be performed to compare monolayer composition resulting from place-exchange vs. codeposition.

5 Appendix

In addition to the two projects discussed previously, I have worked with Professor Rein Kirss at Northeastern University to examine the catalytic behavior of several ruthenium metal complexes. $CpRu(PPh_3)_2X$ (where X = F, Cl, Br, $SnCl_3$ or SnF_3) compounds are useful catalysts in the conversion of methanol to methyl acetate.[54] The proposed mechanism involves substitution for PPh_3 as the rate-determining step. The goal of this project was to measure the rate of PPh_3 substitution to determine the effect of X on the reaction rate. To this end, several compounds were synthesized in which X = Cl, Br, I, SCN, and NCO. Professor Kirss collected kinetic data on these compounds, demonstrating the trend for reaction rate as follows Cl>Br>I>SCN with NCO being a bit faster or a bit slower than Cl. This trend is consistent with a dissociative mechanism, in which PPh_3 is lost followed by the addition of $PMePh_2$ (an 18 electron complex goes to a 16 electron complex by a dissociative pathway). To supplement this data, I performed cyclic voltammetry on all of these samples to determine the standard reduction potential of each compound. Voltammetry was performed in dichloromethane (DCM) with 0.100 M tetrabutylammonium hexafluorophosphate as the supporting electrolyte. A gold microelectrode, a silver wire, and a gold wire were used as the working, reference, and counter electrodes, respectively. To compensate for fluctuations in the reference potential of the silver wire, all measurements were taken in the presence of 1 mM ferrocene. Voltammograms for all samples are shown below:

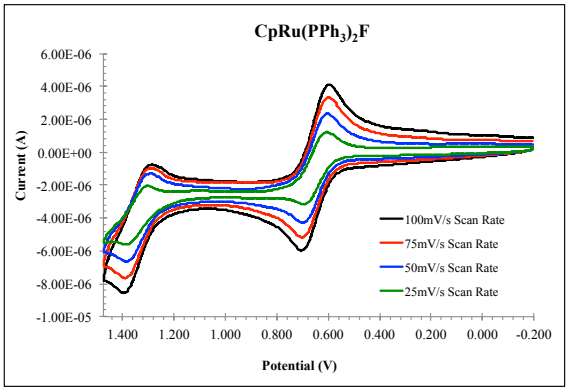
CpRu(PPh3)2F
Current (A)
Potential (V)
100mV/s Scan Rate
75mV/s Scan Rate
50mV/s Scan Rate
25mV/s Scan Rate

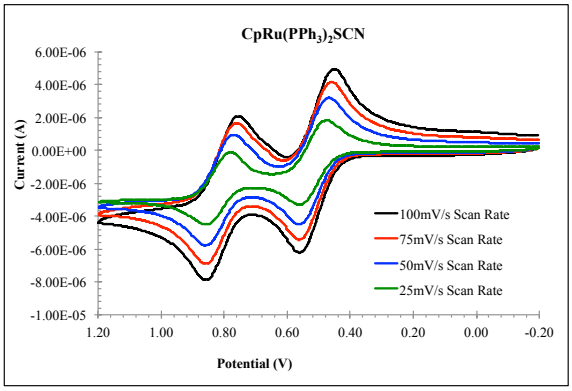
CpRu(PPh3)2SCN
Current (A)
Potential (V)
100mV/s Scan Rate
75mV/s Scan Rate
50mV/s Scan Rate
25mV/s Scan Rate

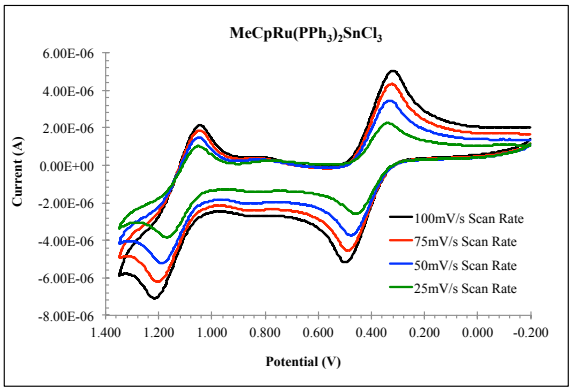
MeCpRu(PPh3)2SnCl3
Current (A)
Potential (V)
100mV/s Scan Rate
75mV/s Scan Rate
50mV/s Scan Rate
25mV/s Scan Rate

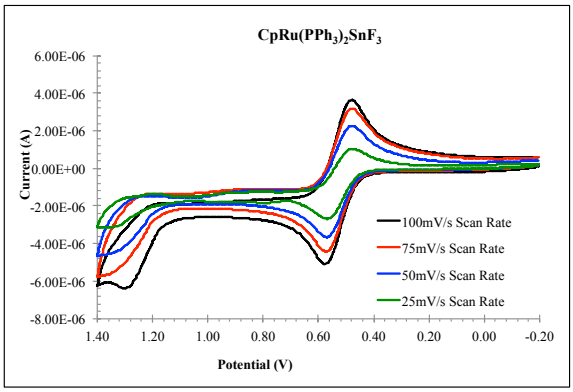
CpRu(PPh3)2SnF3
Current (A)
Potential (V)
100mV/s Scan Rate
75mV/s Scan Rate
50mV/s Scan Rate
25mV/s Scan Rate

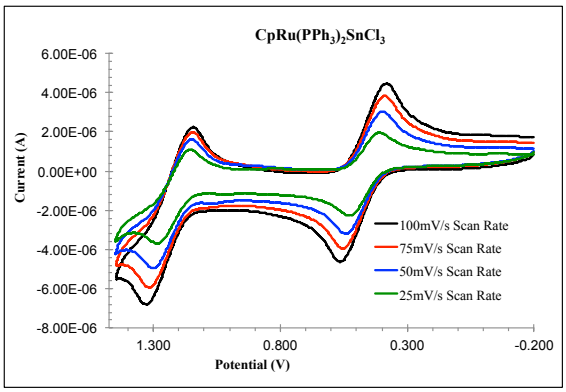
CpRu(PPh3)2SnCl3
Current (A)
Potential (V)
100mV/s Scan Rate
75mV/s Scan Rate
50mV/s Scan Rate
25mV/s Scan Rate

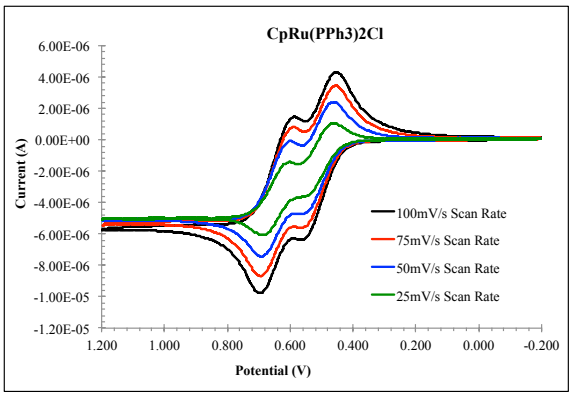
CpRu(PPh3)2Cl
Current (A)
Potential (V)
100mV/s Scan Rate
75mV/s Scan Rate
50mV/s Scan Rate
25mV/s Scan Rate

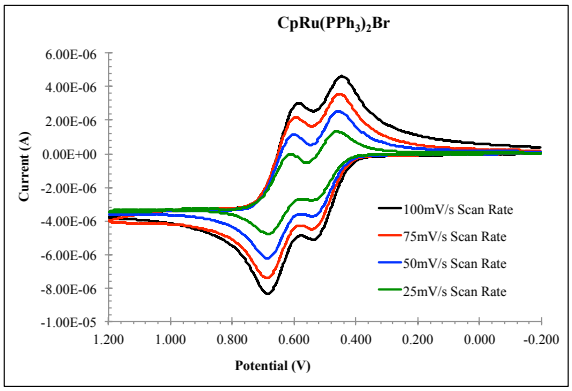
CpRu(PPh3)2Br
Current (A)
Potential (V)
100mV/s Scan Rate
75mV/s Scan Rate
50mV/s Scan Rate
25mV/s Scan Rate

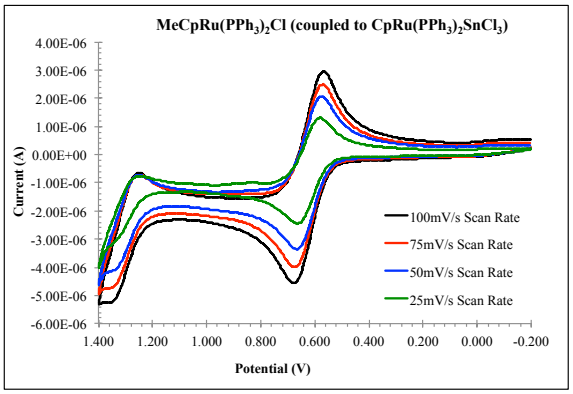
MeCpRu(PPh3)2Cl (coupled to CpRu(PPh3)2SnCl3)
Current (A)
Potential (V)
100mV/s Scan Rate
75mV/s Scan Rate
50mV/s Scan Rate
25mV/s Scan Rate

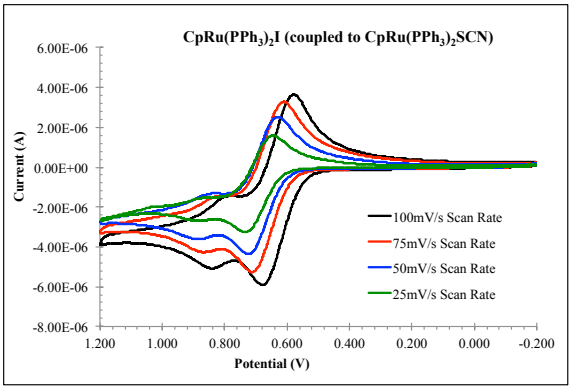

Based on this data, there was a loose correlation between the rate constant for substitution and the standard reduction potential, in addition to the electronegativity of the halide.

A more recent set of experiments involved changing the substituents on the aromatic ring of the phosphine ligand. This is a common practice in tuning the catalytic activity of the complex.[55, 56, 57] Increasing the size of the phosphine ligand is expected to increase the reaction rate. However, increasing size by adding substituents to the phosphine ligand simultaneously affects steric hindrance, which in turn affects the electronic properties of the PPh_3 ligand. By varying the phosphine ligand from $P(p\text{-tol})_3$ to $P(p\text{-MeOC}_6H_4)_3$ to $P(p\text{-FC}_6H_4)_3$, it is possible to study the electronic effect of the phosphine on the rate of substitution. Replacing $P(p\text{-tol})_3$ with $P(m\text{-tol})_3$ will not significantly alter the electronic environment, but it will change the sterics. In this way, the steric effect can be distinguished from the electronic effect. Again, cyclic voltammetry was performed on all samples to determine the electronic environment of the transition metal complexes. Hopefully the standard reduction potential will correlate with the observed reaction rates. Voltammograms for these compounds are shown below:

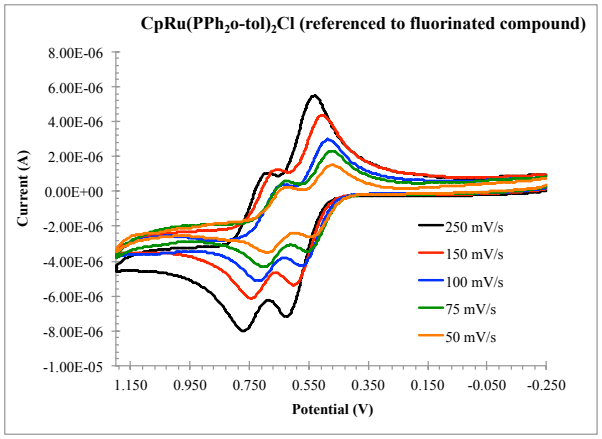
CpRu(PPh2o-tol)2Cl (referenced to fluorinated compound)
Current (A)
Potential (V)
250 mV/s
150 mV/s
100 mV/s
75 mV/s
50 mV/s

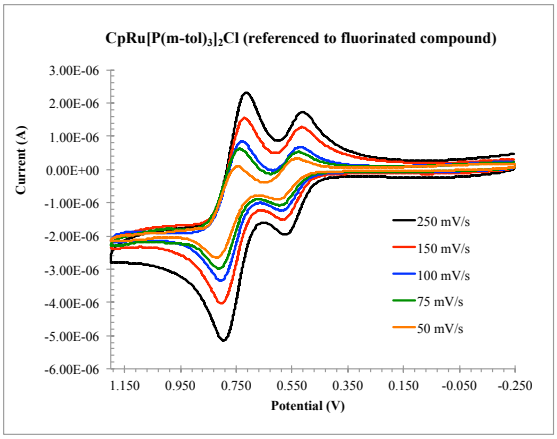
CpRu[P(m-tol)3]2Cl (referenced to fluorinated compound)
Current (A)
Potential (V)
250 mV/s
150 mV/s
100 mV/s
75 mV/s
50 mV/s

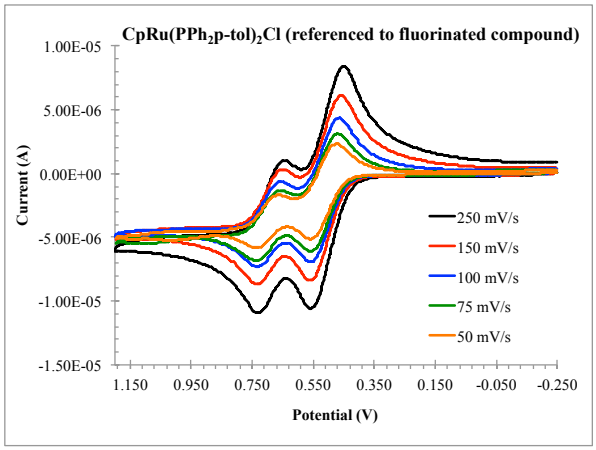
CpRu(PPh2p-tol)2Cl (referenced to fluorinated compound)
Current (A)
Potential (V)
250 mV/s
150 mV/s
100 mV/s
75 mV/s
50 mV/s

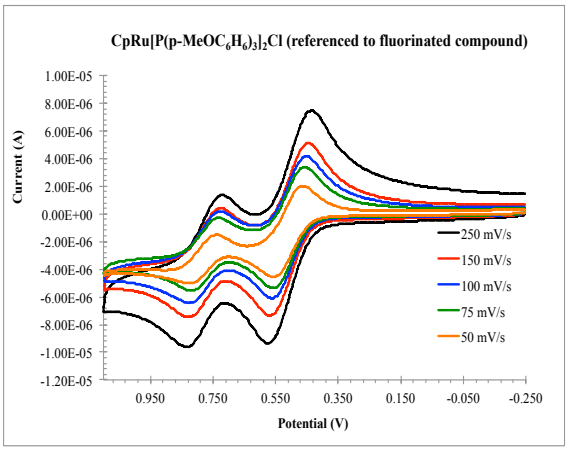
CpRu[P(p-MeOC6H6)3]2Cl (referenced to fluorinated compound)
Current (A)
Potential (V)
250 mV/s
150 mV/s
100 mV/s
75 mV/s
50 mV/s

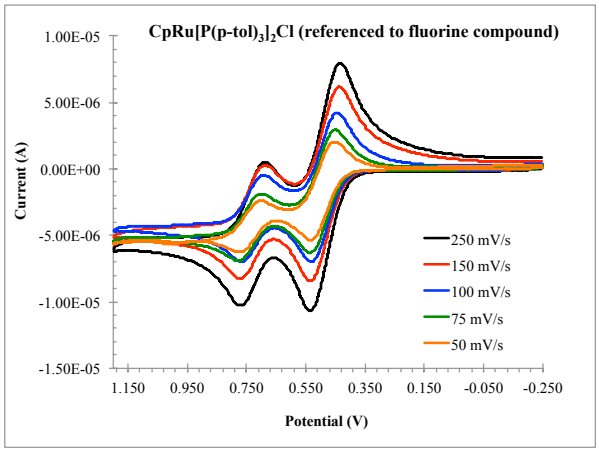
CpRu[P(p-tol)3]2Cl (referenced to fluorine compound)
Current (A)
Potential (V)
250 mV/s
150 mV/s
100 mV/s
75 mV/s
50 mV/s

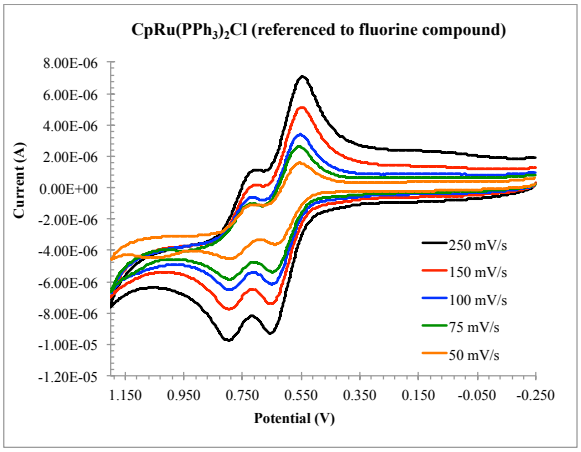
CpRu(PPh3)2Cl (referenced to fluorine compound)
Current (A)
Potential (V)
250 mV/s
150 mV/s
100 mV/s
75 mV/s
50 mV/s

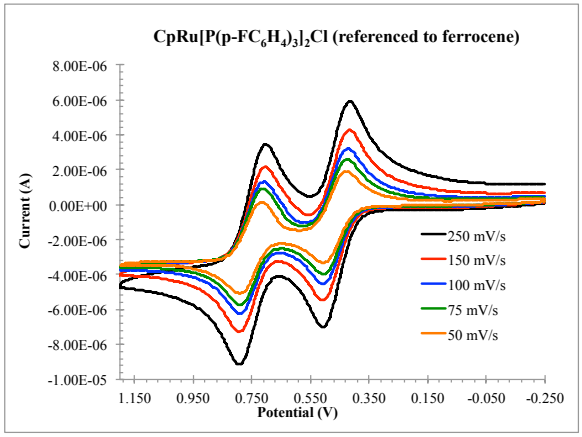

6 References

[1] C. D. Bain, E. B. Troughton, Y. Tao, J. Evall, G. M Whitesides, R. G. Nuzzo, *J. Am. Chem. Soc.* **1989**, 111, 321-335

[2] S Stoeva, J Lee, J Smith, S Rosen, C Mirkin, *J. Am. Chem. Soc.* **2006**, 128, 8378-8379

[3] C Chidsey *Science* **1991** 251, 919-922

[4] Y. Kim, R. Johnson, J. Hupp, *Nano Letters* **2001**, 1, 4, 165-167.

[5] G. Peng, U. Tisch, O. Adams, M. Hakim, N. Shehada, Y. Broza, S. Billan, R. Abdah-Bortnyak, A. Kuten, H. Haick *Nature Nanotechnology* **2009**, 4, 669-673.

[6] L. Authier, C. Grossiord, P. Brossier, B. Limoges, *Anal. Chem.* **2001**, 73, 4450.

[7] C. D. Bain, J. Evall G. M. Whitesides, *J. Am. Chem. Soc.* **1989**, 111, 7155-7164

[8] C. D. Bain, G. M. Whitesides, *J. Am. Chem. Soc.* **1989**, 111, 7164-7175

[9] D. M. Collard, M. A. Fox, *Langmuir*, **1991**, 7, 1192-1197

[10] C. S. Weisbecker, M. V. Merritt, G. M. Whitesides, *Langmuir*, **1996**, 12, 3763-3772

[11] J. Love, L. Estroff, J. Kriebel, R. Nuzzo, G. Whitesides, *Chem. Rev.* **2005**, 105, 1103-1169

[12] M. Brust, M. Walker, D. Bethell, D. Schiffrin, R. Whyman, *J. Chem. Soc. Chem. Coom.*, **1994**, 801-802

[13] E. Chan, M. Yousaf, M. Mrksich, *J. Phys. Chem. A,* **2000**, 104, 9315-9320

[14] M. Yousaf, E. Chan, M. Mrksich, *Angew. Chem. Int. ed*, **2000**, 39, 1943-1946

[15] I. Choi, Y. Chi, *Angew. Chem. Int. Ed.* **2006**, 45, 4894-4897

[16] M. N. Yousaf, B. T. Houseman, M. Mrksich, *Angew. Chem. Int. Ed.* **2001**, 40, 1093-1096

[17] K. Kim, H. Yang, S. Jon, E. Kim, J. Kwak, *J. Am. Chem. Soc.* **2004**, 126, 15368-15369

[18] J. P. Collman, N. K. Devaraj, C. E. D. Chidsey, *Langmuir*, **2004**, 20, 1051-1053

[19] P. A. Bertin, D. Georganopoulou, T. Liang, A. L. Eckermann, M. Wunder, M. J. Ahrens, G. F. Blackburn, T. J Meade, *Langmuir*, **2008**, 24, 9096-9101

[20] C. Chidsey, C. Bertozzi, T. Putvinski, A. Mujsce, *J. Am. Chem. Soc.* **1990**, 112, 4301-4306

[21] D. Collard, M. Fox, *Langmuir*, **1991**, 1192-1197

[22] A. Larson, K. Gothelf, *Langmuir***, 2006**, 21, 1015-1021

[23] H. O. Finklea, D. D. Hanshew, *J. Am. Chem. Soc.,* **1992**, 114, 3173-3181

[24] H. Hong, W. Park, *Langmuir*, **2001**, 17, 2485-2492

[25] Bard, A. J.; Faulkner, L. R. *Electrochemical methods : fundamentals and applications;* 2nd ed.; Wiley: New York, 2001.

[26] E. Katz, A. An. Shipway, I. Willner, *Nanoscale Mater*. **2003**, 5-78

[27] M. Franke, T. Koplin, U. Simon, *Small*, **2006**, 2, 36-50

[28] G. Peng, U. Tisch, O. Adams, M. Hakim. N. Shehada, Y. Broza, S. Bilan, R. Abdah-Bortnyak, A. Kuten, H. Haick, *Nat. Nano.* **2009**, 4, 669-673

[29] A. Labande, J. Ruiz, D. Astruc, *J. Am. Chem. Soc.* **2001**, 124, 1782-1789

[30] J. A. Creighton, D. G. Eadon, *J. Am. Chem. Soc. Faraday Trans.* **1991**, 87, 3881-3891

[31] Y. Kim, R. Johnson, J. Hupp, *Nano Lett*, **2001**, 1, 165-167

[32] B. Jordan, C. Subramani, V. Rotello, *Electrochemistry of Functional Supramolecular Systems*, Ch. 11, 301-331 **2010**

[33] A. N. Shipway, M. Lahav, R. Blonder, I. Willner, Chem. Mater. 1999, 11, 13.

[34] L. Authier, C. Grossiord, P. Brossier, *Anal. Chem.* **2001,** 73, 4450-4456

[35] C. Loweth, W. Caldwell, X. Peng, A. Alivisatos, P. Schultz, *Angew. Chem. Int. Ed.* **1999**, 38, 1808-1812

[36] S. Connoly, D. Fitzmaurice, *Adv. Mater.* **1999**, 11, 1202-1205

[37] M. Stevens, N. Flynn. C. Wang, D. Tirrell, R. Langer, *Adv. Mater*, **2004**, 16, 915-918

[38] E. Chan, M. Yousaf, *J. Am. Chem. Soc.* **2006**, 128, 15542-15546

[39] S. Lin, Y. Tsai, C. Chen, C. Lin, C. Chen, *J. Phys. Chem. B.* **2004**, 108, 2134-2139

[40] X. Han, J.Goebl, Z. Lu, Y. Yin, *Langmuir*, **2011**, 27, 5282-5289

[41] M. Brust, M. Walker, D. Bethell, D. Schiffrin, R. Whyman, *J. Am. Chem. Soc. Chem Commun.* **1994**, 801-802

[42] N. T. Flynn, A. A. Gewirth, *J. Ram. Spec.,* **2002**, 33, 243-251

[43] H. Jans, T. Stakenborg, K. Jans, B. Van de Broek, S. Peeters, K. Bonroy, L. Lagae, G. Borghs, and G. Maes, *Nanotechnology*, **2010**, 21, 1-8

[44] S. Link, M. A. El-Sayed, *J. Phys. Chem B.* **1999**, 103, 8410-8426

[45] D. V. Leff, P. C. Ohara, J. R. Heath, W. M. Gelbart, *J. Phys. Chem.* **1995**, 99, 7036-7041

[46] J. Zhou, J. Ralston, R. Sedev, D. A. Beattie, *J. of Colloid and Interface Sci.* **2009**, 251-262

[47] M. Hostetler, A. C. Templeton, R. W. Murray, *Langmuir*, **1999**, 15, 3782-3789

[48] L. J. Reed, B. G. DeBusk, I. C. Gunsalus, G. H. F. Schnakenberg, *J. Am. Chem. Soc.* **1951,** 73, 5920

[49] D. Wang, R. J. Nap, I. Lagzi, B. Kowalczyk, S. Han, B. A. Grzybowski, I. Szleifer, *J. Am. Chem. Soc.*, **2011,** 133, 2192-2197

[50] H. Soo Choi, W. Liu, P. Misra, E. Tanaka, J. P. Zimmer, B. Itty Ipe, M. G. Bawendi, J. V. Frangioni, *Nat. Biotech.* **2007**, 25, 1165-1170.

[51] J. Eliassaf, *J. Appl. Polym. Sci*., **1978**, 22

[52] H. Schild, M. Muthukumar, D. Tirrell, *Macromolecules*, **1991**, 24, 948-952

[53] H. Biebuyck, G. M. Whitesides, N. Jeon, R. G. Nuzzo, *Langmuir*, **1995**, 11, 4371-4382

[54] P. A. Robles-Dutenhefner, E. M. Moura, G. J. Gama, H. G. L. Siebald, E. V. Gusevskaya, *J. Mol. Cat. A.* **2000**, 164, 39-47

[55] B. M. Trost, Y. H. Rhee, *J. Am. Chem. Soc.* **2002,** 124, 2528-2533

[56] W. Baratta, W. A. Herrmann, R. M. Kratzer, P. Rigo, *Organometallics*, **200**, 19, 3664-3669

[57] F. E. Kuhn, A. M. Santos, A. A. Jogalekar, F. M. Pedra, P. Rigo, W. Baratta, *J. Cataly.* **2004**, 227, 253-256.